

**Cloud Lidar research at the Royal
Netherlands Meteorological Institute
and KNMI2B2 version 2 Cloud Lidar
analysis software documentation**

by

*Alexandre Y. Fong and
André C.A.P. van Lammeren*

Technical report; TR-172

De Bilt 1994

Postbus 201
3730 AE De Bilt
Wilhelminalaan 10
Telefoon 030-206 911
Telefax 030-210 407

UDC: 551.501. 776
551.501.816
681.3.06

ISSN: 0169-1708
ISBN: 90-369-2067-1

© KNMI De Bilt. Niets uit deze uitgave mag worden verveelvoudigd en/of openbaar gemaakt worden door middel van druk, fotocopie, microfilm, of op welke wijze dan ook zonder voorafgaande schriftelijke toestemming van het KNMI.

**Cloud Lidar Research at The Royal
Netherlands Meteorological Institute and
KNMI2B2 Version 2 Cloud Lidar Analysis
Software Documentation**

**Alexandre Y. Fong
and
André van Lammeren**

October 1994

Document Description

Clouds are without a doubt a critical piece in the climatological puzzle. Specifically, the interaction between clouds and radiation form a linchpin in fundamental understanding of both the Earth's hydrological as well the radiative budgets. The Tropospheric Energy and Water Budget Experiment (TEBEX) being performed by the Atmospheric Research Section of the KNMI is motivated by this interest. TEBEX combines an extensive set of observations from satellite, and passive and active ground-based sensors with input from modellers. The goal is gain detailed insight into a $130 \times 130 \text{ km}^2$ area covered by 10 ground observation sites know as the Cloud Detection System (CDS). Further details of the CDS program in its entirety are given elsewhere [1].

The objective of the KNMI-TEBEX Lidar component are to obtain a set of cloud optical and physical data as derived by lidar for comparison and analyses with satellite data in a research aimed at exploring the Earths Radiation Budget (ERB). To that end, software has been developed to process such lidar measurements to obtain the salient information. This information includes: cloud base and top height, peak signal altitude, physical thickness, optical extinction and depth.

KNMI2B is a software package specifically created for the analysis of lidar (laser-radar) data obtained from the National Institute of Public Health and Environmental Protection (RIVM) Laboratory for Air Quality Research aerosol lidar system in Bilthoven, The Netherlands for use by the Royal Netherlands Meteorological Institute (KNMI) in De Bilt, The Netherlands.

This study was contracted as part of a scientific consulting contract on cloud lidar studies by Dr. André Van Lammeren of The KNMI. The software was designed and authored by Mr. Alexandre Y. Fong as per Dr. Van Lammeren's requirements and specifications. Ownership of this software is shared by Dr. Van Lammeren, Mr. Fong and The KNMI. These parties assume no liability for damage to devices or existing software that may result from its subsequent use.

KNMI2B incorporates widely used algorithms and definitions to derive optical and physical properties of interest and insight to those studying the effects and contributions of cloud to climate and atmosphere. The source code is written in Microsoft FORTRAN 5.1 and incorporates an algorithm developed by the Institute for Space and Terrestrial Science (ISTS) in Toronto, Ontario, Canada by Dr.'s Allan I. Carswell, Shiv R. Pal, Wolfgang Steinbrecht.

KNMI2B obtains the following parameters:

- Cloud Base Altitude
- Cloud Peak Signal Return Altitude
- Apparent Cloud Top
- Mid-Cloud Altitude
- Cloud Mean Optical Extinction [calculated from both the integrated Klett inverted extinction profile and by comparing the above and below cloud background]
- Optical Extinction (profile)
- Optical Depth

KNMI2B2 also identifies and obtains cloud base height algorithm information but can, if the operator chooses to, disregard inverting saturated profiles for optical data. KNMI2B also provides output that has sonde information correlated to cloud base height optical and physical information listed above.

Acknowledgements

The author wishes to acknowledge the assistance and cooperation of Eric Visser, Hans Bergwerth, Arnout Apituley and Daan Swart of the National Institute of Public Health and Environmental Protections (RIVM), Laboratory for Air Quality Research.

Special thanks to Dr. André Van Lammeren and Carin, Joris, and Roos Van Lammeren for their kind hospitality and friendship. Special thanks to André for his insight and suggestions which kept the momentum of this work going.

Thanks also Pieter Levelt and Wim Vassen for their friendship and company, Arnout Feijt and Piet Stammes for all their advice and technical assistance with this project, Ronald Weber and Wieger Fransen for making their home mine, Barbara Bongers, Sigrida Shperlina, Ad, Paul and Hanna, and making the bus rides to and from DeBilt shorter, Glenn (like a father to me!), Naci, Baelul, Sunil, Bibi, Lydia, Audrey, Everet, Ron Grovers (thanks for the postcard) and everyone else at Gravenbeek's (the friendliest place in Holland!) and everyone else at the KNMI for making my stay a pleasant one.

Special thanks to the people of Optech Inc.: Adelhied Freitag, Dino Lenarduzzi, Taner Machupyan, Victor Gorin, Martin Flood, Michel Stanier, Larry Mitchel, Jim Bottoms, Rob Murenbeeld and Wayne Sziemetat for keeping me company and up to date on all the great gossip back home, away from home. Thank you to Doug and Lorraine Houston at Optech and Linda and Allan at the Harry Sherman Crowe Co-op for also helping me keep all things residential under control back home.

Very special thanks to Stefan Mihalov, Michel Stanier, Adelhied Freitag, and the Steinbrechts of München for all their kind hospitality in showing me their special parts of Europe. Thanks to Victor Gorin, Bill Dykshoorn and Pam Dillon (*and friend*) for dropping by.

Thanks to all the other folks who sent me email and let me share in their lives this last summer: Paul Fairlie, Dwaine Plaza, Denise, Jan McQuay, Sandra Scott and Dave Tatar.

As always thanks to Dr.'s Allan I. Carswell and Shiv R. Pal for their support and wisdom throughout the years which made all this work possible.

Kudos to all at the *Cirrus Technology Consulting* home office in Toronto for a job well done.

Finally, thank you to as always my parents, for their love and support.

“But trouble can come to nice places, too; trouble travels, trouble visits. Trouble even takes holidays from the places it thrives, from places like St. Cloud’s.”

“What is hardest to accept about the passage of time is that the people who once mattered the most to us are wrapped up in parenthesis.”,
John Irving, *The Cider House Rules*

“Life is what happens when you’re making other plans”,
John Lennon

“...and I am oughta here!”,
Dennis Miller, Weekend Update: Saturday Night Live

©1994, *Cirrus Technology Consulting Press*

Contents

Document Description	iv
Acknowledgements	vi
Table of Contents	viii
List of Tables	x
List of Figures	xi
1 Lidar Fundamentals	1
1.0.1 The Lidar Equation	3
1.0.2 The Volume Backscatter Coefficient	4
1.0.3 The Volume Extinction Coefficient	4
1.0.4 Multiple Scattering	5
1.0.5 Cloud Lidar Measurements	7
1.1 Extinction Coefficient Inversions	7
1.1.1 The Slope Method Extinction Coefficient Inversion	9
1.1.2 Far-End Extinction Coefficient Inversions	10
1.1.3 Direct Effective Mean Extinction Coefficient Inversions	11
1.2 The Cloud Base Height	12
1.2.1 Definition of Cloud Base	13
1.2.2 The Cloud Base Height Algorithm	14
1.3 Data Averaging Techniques	17
2 Inverting Real Lidar Returns: Practical Considerations and Caveats	19
2.1 Data Quality	19
2.2 Practical Application of the Klett Inversion Algorithm	24

2.2.1	Estimations of the Reference Altitude and Extinction	24
2.2.2	Use of Averaging Techniques	34
2.2.3	Example of an Inversion of Real Data	36
3	KNMI2B2 Main Code General Requirements:	39
3.0.4	KNMI2B2 Main Code Operating Description:	39
3.1	KNMI2B2 Operating Requirements: Support Files,Inputs and Formats	44
3.2	KNMI2B2 Input/Output File Formats:	47
3.3	Installing KNMI2B2 and CirrusWare	50
3.4	Tutorial	50
3.5	Examples of KNMI2B2 Outputs:	52
4	Other Software	60
4.1	Lidar Simulation Software Set	60
4.2	Miscellaneous Support Software Included:	64
4.3	Software for Catalyst:	66
5	Conclusions	68
5.1	Diagnosis: Current Condition	68
5.2	Future Plans: Prognosis	69
5.2.1	Other Improvements: Far-End Extinction Coefficient In- versions with Range Variable Backscatter to Extinction Ratios	73

List of Tables

2.1	Technical Overview of the RIVM Truck Mounted Nd:YAG 1064 nm, 70 mJ Aerosol Boundary Layer Lidar System	23
5.1	Comparison of Moisture Detection Capabilities Between the KNMI Cabauw Meteorological Tower and a potential Raman Water Vapour Lidar	70
5.2	Comparison of Moisture Detection Capabilities Between the KNMI Cabauw Meteorological Tower and a potential Raman Water Vapour Lidar, continued.	71

List of Figures

1.1	Schematic of the monostatic, biaxial lidar configuration utilized. The laser and telescope comprise the transmitter and receiver, x is the overlap range.	2
1.2	Schematic representation of lidar beam behavior in a turbid medium [32]	6
1.3	Schematic of cloud base algorithm	16
2.1	expected lidar signal return at $1064nm$ calculated by assuming a pure Rayleigh atmosphere as a attenuating and backscattering medium, calibrated and plotted with the data from a cloudless sky on August 4th, 1993 from the RIVM lidar system	20
2.2	Lidar backscatter profiles from August 4th, 1993 [93216], trace 74 (<i>top</i>) and trace 225 (<i>bottom</i>).	22
2.3	Graph showing optical extinction profiles for a pure molecular or Rayleigh atmosphere at $1064nm$. Generated using sonde measurements (—) and using an assumed lapse rate of $-6.5^{\circ}C/km$ and the hydrostatic pressure equation (---)	25
2.4	Simulated relative range-corrected logarithmic lidar backscatter signal ($S - S_0$) for a simulated <i>plateau shaped</i> optical extinction profile	27
2.5	Klett inversions of the previous simulated backscatter profile figure using varying values for the reference optical extinction boundary condition, σ_f	28
2.6	Klett inversion of a simulated constant extinction profile using varying values of σ_f	29
2.7	Klett inversion of a simulated constant extinction profile using varying values of reference height signals.	30
2.8	Klett inversion of a simulated constant extinction profile with varying constant values added and subtracted to the entire profile.	31

2.9	Graph of range at which varying the reference optical extinction value, reference height signal value and constant added or subtracted to the profile effect of the height at which the recovery of the inversion to within 10% of the correct value occurs.	33
2.10	Plot of an original lidar backscatter signal as collected from August 4 1993 [93216] ((.....)). A profile where the value of the most negative signal value is added to the entire profile along with a small offset is also plotted ((---)). Signal values from the top-most range height (4000m) down to 1500m (the height at which we expect to begin to detect some of the background atmosphere) are averaged or fitted to 5 points above and below the signal point of interest and shown as ((——)).	35
2.11	Plot of a range corrected signal (trace 6) from August 4th 1993 [93216]	37
2.12	Inversions of a signal (trace 6) from August 4th 1993 [93216] using a variety of values for the reference extinction coefficient, with and without averaging.	38
3.1	Flow chart of the KNMI2B2 software features and data processing scheme, part 1.	41
3.2	Flow chart of the KNMI2B2 software features and data processing scheme, part 2.	42
3.3	Flow chart of the KNMI2B2 software features and data processing scheme, part 3.	43
3.4	Grey-scale plot showing the backscatter intensity time series of the lidar returns for the day 93216 (August 4th, 1993) without range correction (files 93216nrc.dat)	54
3.5	Plot of the file 93216clb.dat, indicating the detected cloud base, peak signal return height and apparent cloud top height for the day 93216 (August 4th, 1993)	55
3.6	Grey-scale plot of the optical extinction derived from the backscatter intensity, for the day 93216 (August 4th, 1993), using the Klett Inversion	56
3.7	Time-series of the optical depth generated from the 93216op2.dat file	57
3.8	Scatter plot comparing the cloud optical depths generated from both 93216op2.dat and 93216tru.dat files	58

3.9 Scatter plot of cloud optical extinction compared with temperature at mid-cloud height 59

Chapter 1

Lidar Fundamentals

A typical atmospheric lidar system is comprised of two major components: a transmitter, (ie. laser source), which sends out a light beam of controlled characteristics through the portion of the atmosphere of interest and a receiver which detects the energy backscattered into it's field-of-view (FOV). This backscattered signal contains information on the scattering and absorption processes taking place within that portion of atmospheric medium probed by the beam. If the lidar-atmosphere interactions are understood then an inference can be made as to the composition or condition of the atmosphere. With short pulse laser sources the time of flight of the return pulse provides excellent range resolution.

Two configurations of the transmitter-receiver are utilized in lidar systems. The bistatic configuration places the transmitter and receiver at different locations. All of our work has been performed on the more common monostatic configuration, where the transmitter and receiver are located together. Our monostatic system has the transmitter and receiver axes aligned collinearly. Fig. 1.1 is a schematic of this configuration. Monostatic lidar consequently relies upon measurement of energy scattered at 180° from the incident beam source. By utilizing a laser source with short pulse lengths, high repetition rates and large energies, and consequently high average power, weak interaction phenomena at distant ranges can be examined with high spatial resolution and good signal-to-noise ratios (SNRs).

The overlap range, x , is defined as the range at which there is full overlap of the receiver FOV with the transmitter beam. Beyond this range the signal decreases inversely as the square of the distance in a homogeneous atmosphere. At closer ranges the backscatter intensity increases rapidly as the transmitter's beam falls within the receiver's FOV. This intense region of backscatter is often

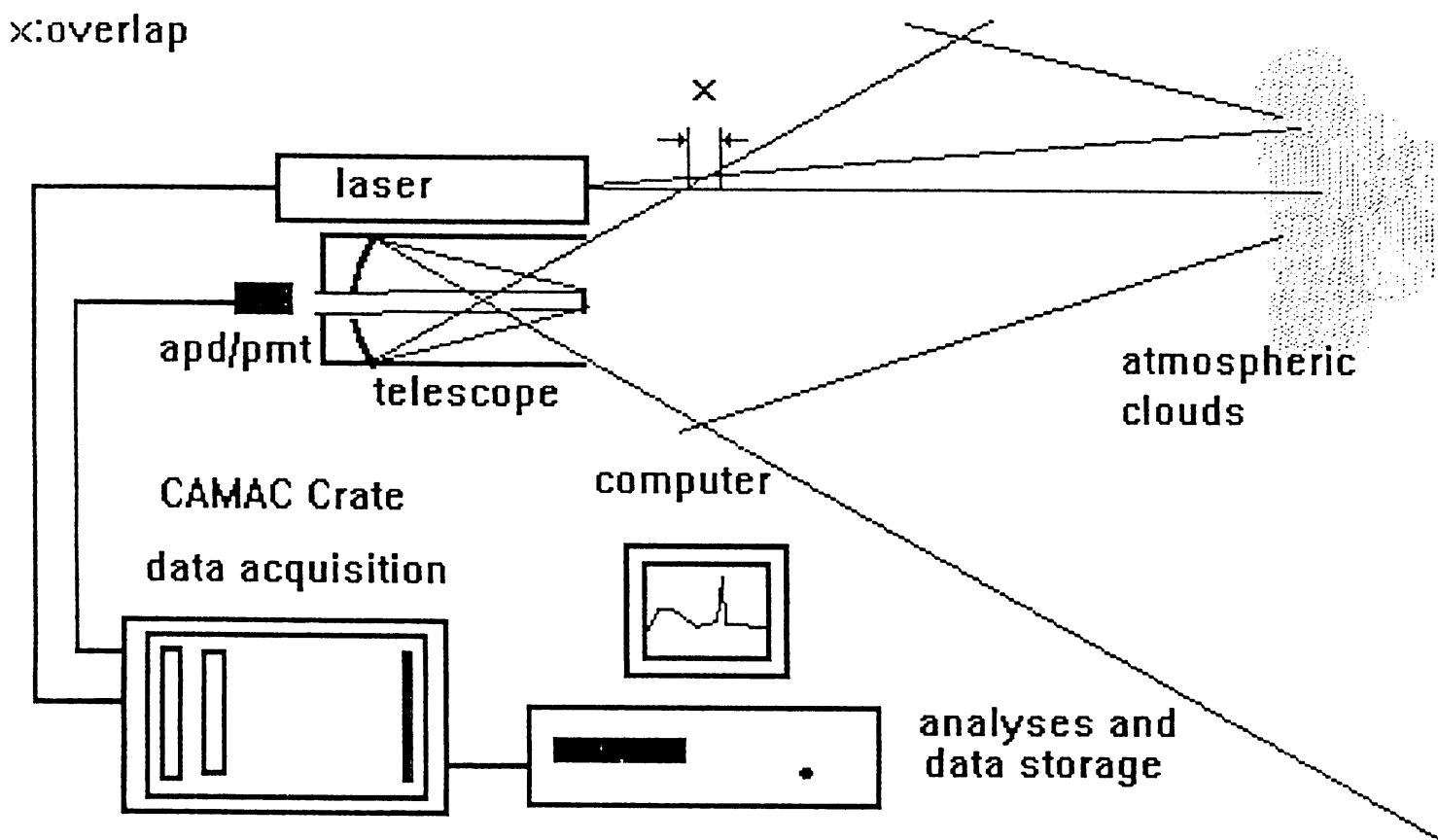


Figure 1.1: Schematic of the monostatic, biaxial lidar configuration utilized. The laser and telescope comprise the transmitter and receiver, x is the overlap range.

suppressed in many lidar configurations to reduce demands on the detector's dynamic range.

For the lidar system we are concerned with, this portion of the range lasts for up about 800 m (5 us) and has a maximum signal of over 500 mV (the maximum range of the digitizer). A cloud layer signal (with the current optical attenuation settings on our receiver is about 50 mV). The noise level is about 1-2 mV.

Please note the two-way path involved in the time/distance discussion above.

1.0.1 The Lidar Equation

If only single scattering events are assumed to redirect the photons to the receiver as they travel through their atmospheric path then the well known lidar equation can be considered valid [2]:

$$P(r) = P_0 \frac{c\tau}{2} \frac{A\beta(r)}{r^2} e^{[-2 \int_0^r \sigma(r') dr']} \quad (1.1)$$

Where,

τ = the pulse duration

$P(r)$ = the instantaneous received power from range r
at time t

P_0 = the transmitted power at time t_0

c = the velocity of light

A = the effective system receiver area

r is the range [= $\frac{c(t-t_0)}{2}$]

$\beta(r)$ is a measure of the incident laser power backscattered by the atmosphere per solid angle and per unit path length and is known as the volume backscatter coefficient.

$\sigma(r)$ is the signal attenuation per unit length from the lidar beam due to the scattering and absorption of the incident radiation and is known as the attenuation or extinction coefficient.

The nominal vertical (spatial) resolution of lidar ($\Delta z = c\tau/2$) is determined by the length of the laser pulse. The horizontal resolution is a function of the beam divergence. Current laser systems are capable of producing pulse durations on the order of 10ns, as is the case for our system. Furthermore beam divergences are typically on the order of 1mrad. This results in spatial resolution unattainable by any other atmospheric remote sensing technique.

1.0.2 The Volume Backscatter Coefficient

The fractional amount of incident energy scattered per steradian back into the receiver per unit path length is given by the volume backscatter coefficient, β . The β has units of $m^{-1}sr^{-1}$ and is the result of scattering contributions from all atmospheric constituents. β is often expressed as,

$$\beta = \sum_i \beta_i = \sum_i N_i d\Sigma(\pi)_i / d\Omega \quad (1.2)$$

for all i atmospheric scattering species with number density N_i , and backscatter cross section $d\Sigma(\pi)_i / d\Omega$. The latter varies in magnitude from the order of $10^{-8}cm^2sr^{-1}$ for aerosol particles to below $10^{-28}cm^2sr^{-1}$ for scattering due to Raman effects. The wavelength dependence of the backscatter cross section also makes β a wavelength dependent quantity [3][2]. The β may also be expressed as the product of the volume scattering coefficient σ_s and the backscatter scattering phase function $\frac{P_\pi}{4\pi}$

$$\beta = \sigma_s \frac{P_\pi}{4\pi} \quad (1.3)$$

1.0.3 The Volume Extinction Coefficient

One of the most fundamental and important optical parameters measured by lidar is the volume extinction coefficient σ , defined as the extinction cross section per unit volume with units of m^{-1} . In the integral in Eq. 1.1, σ represents a summation of all the atmospheric attenuation processes affecting the pulse in its two-way path through the atmosphere. It is most commonly expressed as,

$$\sigma = \sigma_a + \sigma_m + k_a + k_m \quad (1.4)$$

where σ_a and σ_m are extinction coefficients due to scattering from atmospheric aerosol and molecular constituents, respectively. k_a and k_m are similarly the aerosol and molecular extinction coefficients resulting from atmospheric absorption. k_m is strongly wavelength dependent in comparison to the other coefficients. At many wavelengths, strong molecular absorption limits the propagation of the transmitter signal and hence the utility of lidar. Careful selection of incident frequencies within the so-called *atmospheric windows*, where k_m is negligible, provides a remedy to this problem [3][2].

For studies of clouds, $\sigma_a \gg \sigma_m$ and we need only consider a single term, σ , resulting from the scattering of the cloud particles. Related quantities of cloud

depth and mean volume extinction coefficient also are often useful. In terms of the volume extinction coefficient we define the optical depth of the cloud as,

$$\tau = \int_{r_b}^{r_t} \sigma(r) dr \quad (1.5)$$

Given cloud base and top altitudes, (r_b and r_t , respectively), the *mean volume extinction coefficient* for the cloud may then be defined as,

$$\bar{\sigma} = \tau / (r_t - r_b) \quad (1.6)$$

[4].

1.0.4 Multiple Scattering

Equation 1.1 is less representative of backscattering in cases of higher turbidity where multiple scattering effects dominate. Such is the case for dense clouds and certain atmospheric aerosols.

Fig. 1.2 is a very simplified illustration of the contributions from multiple scattering to the backscatter in turbid media. As the beam enters into the cloud the beam is broadened by forward scattering due to the cloud droplets. The three regions: A, B and C represent the continuation of the original beam, the broadened beam still in the receiver's field FOV and outside the receiver's FOV, respectively. Region A is predominantly the result of single scattering whereas B and C are strictly due to multiple scattering; the latter being the result of at least the initial scattering incident and subsequent events redirecting the photons back into the receiver's FOV. In actuality, photons may undergo many more scatterings within and outside the receivers FOV making the problem all the more complex [5].

The degree of multiple scatter is a function of two main processes: the angular dependence of the scattering and the rate at which multiple scattering occurs. These are dictated by the medium's composition, scatterer optical properties and number densities. However, the measured contribution to multiple scattering is also dependent upon the beam divergence and the target medium's range from the lidar. Any multiple scattering lidar equation will necessarily be more complex than in Eq. 1.1 [6] [7].

Efforts to include such effects remain an active field of inquiry. At present there exists no widely accepted modification of Eq. 1.1 which adequately includes multiple scattering effects. Several radiative transfer model approximations as

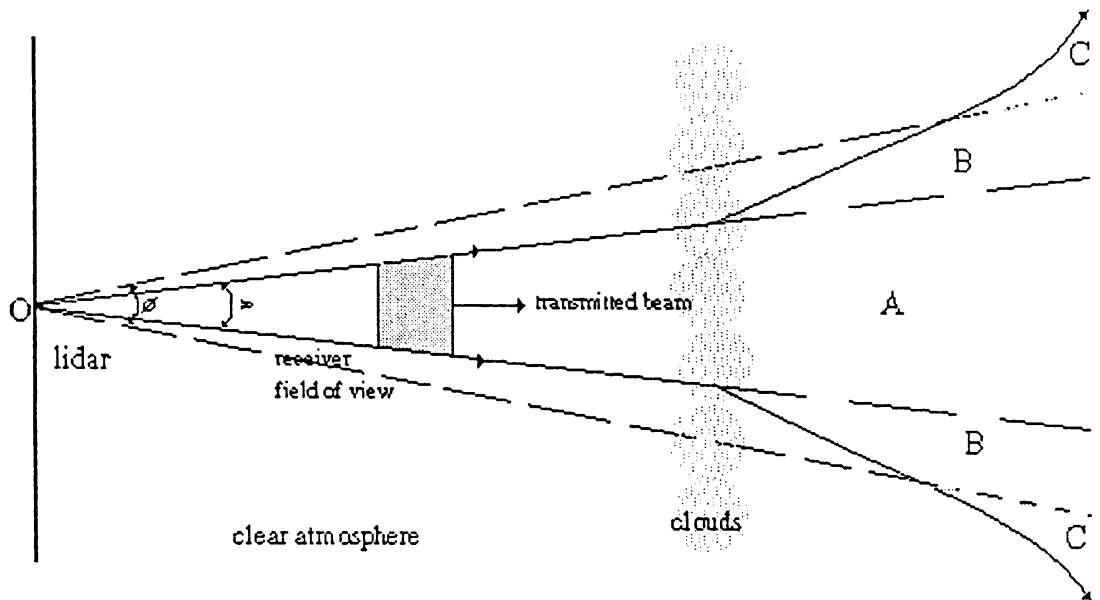


Figure 1.2: Schematic representation of lidar beam behavior in a turbid medium [32]

well as time dependent multiple scattering models have been developed [8][9][10]. The advent of low cost, high speed computing platforms have permitted some advances but at present there exists no adequate atmospheric radiative transfer models which fully account for multiple scattering in the lidar equation. The spatial ambiguity of the scattering volume due to multiple scattering also degrades the time-dependent range resolution of lidar since there is no longer a direct proportionality between the distance to the scattering volume and the time of flight of the pulse.

1.0.5 Cloud Lidar Measurements

Due to the large scattering cross-sections of the particles involved, clouds induce large backscatter. As mentioned above the effects of multiple scattering can introduce difficulties into the interpretation of some lidar cloud *signatures*. By noting the lidar signal from the atmosphere above the cloud, one can determine the level of signal penetration of the beam. This aspect is particularly important to ensure that lidar has penetrated low-level dense clouds composed primarily of water droplets [3][2]. However, there are many of these clouds for which the lidar probing range is only one or two hundred metres. Thus lidar data are limited by the ability of the beam to penetrate the cloud.

Lidar excels at defining cloud spatial distribution, particularly cloud base altitudes and geometric thicknesses. This has spawned the development of commercial ceilometer instruments for the routine monitoring of cloud bases for use in aviation [11]–[13]. Although the inversion of lidar returns for the purpose of extracting atmospheric optical parameters presents challenges, lidar offers measurement of such quantities with unparalleled temporal and spatial resolution. In clouds, the lidar scattering signature is an indicator of a cloud’s interaction with solar radiation[3][14]. The combination of lidar and narrow beam radiometer measurements (*LIRAD*) has shown much success in furthering our knowledge of cloud radiative properties [15] –[20].

1.1 Extinction Coefficient Inversions

The reliable extraction of attenuation and backscatter parameters from lidar returns by inversion methods has been a long standing and relatively unfulfilled goal of lidar researchers. A number of factors, ranging from technological limitations to theoretical constraints, have prevented the successful development of

satisfactory inversion processes. Particular interest has been given to obtaining accurate values of the volume extinction coefficient for reasons discussed in Sec. 2.1.2.

The *Inverse Problem* is central to all optical remote sensing techniques. As is clear from Eq. 1.1, the observable P is dependent upon a number of parameters. Most are system dependent and as such can be determined in a relatively direct manner. The two atmospheric parameters, β and σ , must be determined by solving or “inverting” the equation. Both parameters are unique to the particular atmospheric optical situation we are attempting to determine. This one-to-many mapping from P to these atmospheric parameters results in an infinite number of combinations for the inversion solution. Such an inverse problem is thus ill-posed or underdetermined.

To proceed, what is required are some constraints to limit the possible solution set, and to reduce the underdetermination of this problem. In one approach, many measurements of P are obtained with a controllable varying parameter such as incident wavelength or beam angle. With the resultant simultaneous equations the problem becomes solvable. Such schemes often require complex measurement methods and even so, are subject to the stringent limitations of the assumptions utilized.

For inversions of monochromatic monostatic lidar where one has only a single measurement of P , it is necessary to add some additional information, usually in the form of an assumed functional relationship between the unknowns, β and σ . There is physical basis for this assumption, however in this report no attempt is made to describe this in detail. [21].

Conventionally, the isotropic backscatter-to-extinction ratio has been defined as [4]:

$$C = \beta(\pi, z)/\sigma(z)^k \quad (1.7)$$

where $\beta(\pi, z)$ is the volume backscatter coefficient and $\sigma(z)$ is the volume extinction coefficient. Eq. 1.7, with $k = 1$, is widely used to permit the solution of Eq. 1.1 [21].

Despite these considerations, an impressive arsenal of approaches have been developed by workers. Although, in general, all these techniques have limitations, some can be applied with a large degree of confidence subject to specific instances.

1.1.1 The Slope Method Extinction Coefficient Inversion

The simplest algorithm for the procurement of extinction values from lidar measurements is the so-called slope method. With reference to Eq. 1.1, the lidar equation, we first define $S(r)$ as the 'logarithmic range adjusted power'.

$$S(r) = \ln[r^2 P(r)] \quad (1.8)$$

Rewriting Eq. 1.1 with this new variable it can now be expressed as,

$$S - S_0 = \ln\left(\frac{\beta}{\beta_0}\right) - 2 \int_{r_0}^r \sigma dr' \quad (1.9)$$

Where $\beta_0 = \beta(r_0)$.

The differential form of this equation is:

$$\frac{dS}{dr} = \frac{1}{\beta} \frac{d\beta}{dr} - 2\sigma \quad (1.10)$$

As we have discussed, the solution of this equation requires knowledge of the relationship between β and σ when $d\beta/dr \neq 0$. In the case of a homogeneous atmosphere $d\beta/dr = 0$ and $\sigma = -\frac{1}{2} \frac{dS}{dr}$. Thus the attenuation coefficient may be obtained from the slope of an $S(r)$ versus r plot.

By use of a straight line least squares fitting to the function $S(r)$, $\frac{dS}{dr}$ can be derived over small intervals over which the atmosphere can be considered to be approximately homogeneous with range. The slope method is therefore not considered a profile-resolving technique, as the extinction values are actually estimates of finite intervals.

This method can be applied under actual atmospheric conditions in so far as an interval small enough to be truly said to be homogeneous can be achieved. This is limited by the temporal and spatial resolution of the system used. As such, it also degrades this resolution by its very nature, one of the primary assets of the lidar technique. Signal noise adds yet another complication to this technique. To overcome the effects of noise the chosen interval must be extended. This again leads to a degradation of the spatial resolution of the measurement.

This method also requires the restriction $\beta^{-1} |d\beta/dr| \ll 2\sigma$ to hold throughout most of $S(r)$. Such rare quasi-homogeneous conditions exist in a few dry climates, but is unfortunately not the case for most atmospheric conditions of interest. It is particularly untrue of certain unstable and turbid media, such as dense clouds, fog, smoke and dust. Furthermore, in many stable less turbid

media such as cirrus clouds, spatial variations lead to sharp variances in $d\beta/dr$. Such situations lead to an invalidation of this method [3][21].

1.1.2 Far-End Extinction Coefficient Inversions

A profile-resolved technique requires an “exact” analytical solution. Proceeding from the previously discussed assumed relation given in Eq. 1.7.

We can rewrite Eq. 1.10 in a form corresponding to the Bernoulli or homogeneous Ricatti equation:

$$\frac{dS}{dr} = \frac{k}{\sigma} \frac{d\sigma}{dr} - 2\sigma \quad (1.11)$$

Which has the solution:

$$\sigma = \frac{e^{\frac{1}{k}(S-S_0)}}{[\sigma_0^{-1} - \frac{2}{k} \int^r e^{\frac{1}{k}(S-S_0)} dr]} \quad (1.12)$$

This is commonly known as the ‘near-end’ or ‘forward inversion’. This solution requires knowledge of σ_0 the boundary condition of the extinction coefficient in the near field (close to the lidar). However, the difference of terms in the denominator leads to mathematical instability. The resulting solution is exceptionally prone to noise. These instabilities also propagate and grow as the inversion iterates with range.

One can modify this solution in order to avoid such difficulties using an approach suggested by J.D.Klett [21]. If we define $\sigma(r_f) = \sigma_f$, Eq. 1.12:

$$\sigma = \frac{e^{\frac{1}{k}(S-S_f)}}{[\sigma_f^{-1} + \frac{2}{k} \int^r e^{\frac{1}{k}(S-S_f)} dr]} \quad (1.13)$$

This ‘far-end’ or reverse iteration inversion is often referred to as the ‘Klett Inversion’. The sum in the denominator results in significantly improved stability over the near-end solution. The form of the denominator also indicates that the dependence of the solution on σ_f decreases with increasing range values. By far the most widely used inversions in lidar research are numerical implementations of Eq. 1.13. In our work we have adopted this approach.

The above inversion can be recast by means of the identity $\exp^{\ln x} = x$ into the form,

$$\sigma = \frac{P(r) \times r^2}{\left[\frac{P(r_f) \times r_f^2}{\sigma_f} + \frac{2}{k} \int^r P(r) \times r^2 dr \right]} \quad (1.14)$$

As suggested by Steinbrecht and Visser [22][23]. The advantage gained here, is that this inversion is defined for signal values of ≤ 0 . The definition of the logarithmic range adjusted power, Eq. 1.8, which is used in the Klett inversion, Eq. 1.13, clearly does not permit this. Although Eq. 1.13 and Eq. 1.14 are mathematically identical, in our work it appears not to be the case computationally from our experience with real and simulated data. The author is unable to account for these discrepancies at this time.

Fortunately one can circumvent the problem of values ≤ 0 in several ways as we will discuss later.

1.1.3 Direct Effective Mean Extinction Coefficient Inversions

A value for the cloud optical thickness and subsequently the mean value for the cloud extinction may be derived by comparing the difference in the background return signal from the surrounding atmosphere above and below the cloud. This ratio of the background signal just below the cloud base and just above cloud top is logarithmically proportional to the optical depth of the cloud. This requires the cloud be located in a relatively homogeneous region of the atmosphere and thus the background scattering from above and below the cloud differs only by the two way attenuation by the cloud of the above-cloud return.

The signal at the cloud base can be expressed as:

$$P(r_b) = P_0 \frac{c\tau}{2} \frac{A\beta(r_b)}{r_b^2} e^{-2[\int_0^{r_b} \sigma_A(r) dr]} \quad (1.15)$$

Where the parameters are as previously defined and with the subscript b denoting the atmosphere just below cloud base. σ_A is the mean attenuation of the atmosphere below the cloud.

Similarly for the return from the atmosphere just above cloud top:

$$P(r_t) = P_0 \frac{c\tau}{2} \frac{A\beta(r_t)}{r_t^2} e^{-2[\int_0^{r_b} \sigma_A(r) dr + \int_{r_b}^{r_t} \sigma_C(r) dr]} \quad (1.16)$$

where, σ_C is the mean cloud extinction coefficient.

Defining the scattering ratio:

$$R_{SC} = \frac{P(r_b)}{P(r_t)} = \frac{\beta_b r_b^2}{\beta_t r_t^2} e^{2[\int_{r_b}^{r_t} \sigma_C(r) dr]} \quad (1.17)$$

We may then express the optical depth for the cloud as:

$$\tau_C = \int_{r_b}^{r_t} \sigma_C(r') dr' = \frac{1}{2} \ln\left(\frac{P(r_b)r_t^2}{P(r_t)r_b^2}\right) \quad (1.18)$$

Where we assume $\beta_t \sim \beta_b$ for a homogeneous surrounding atmosphere.

This method has the obvious advantage that it utilizes only those returns that contain cloud signal and does not require a profile of clear air either before or after the cloud moves into the field of view in comparison to similar methods used elsewhere [24]. This has obvious statistical advantages in our confidence of the derived extinction. In practical applications a Rayleigh background atmosphere is assumed from temperature and pressure conditions obtained from sonde launchings.

Such a technique does not provide a complete profile of cloud extinction as is the case for far-end inversions. However, it does not require additional information on the boundary condition and has been found to provide a reliable value for the mean cloud extinction.

1.2 The Cloud Base Height

Among the cloud parameters specified in GCM's, the altitude and thickness information are most important. Cloud base altitudes relate directly to cloud formation and frequency. Emission temperatures can be established given knowledge of cloud base altitudes. Cloud elevation can provide insight into the distribution of atmospheric water vapor. Infrared fluxes are modified by cloud droplet scattering and water vapor absorption. Such information is essential to a better understanding of radiative processes in cloudy atmospheres.

Cloud base height* is also an indicator of a cloud's role as an atmospheric radiation feedback mechanism in the "greenhouse effect". For example, Ohring and Adler [26] have shown that a one kilometre increase in cloud top altitude and subsequently vertical extent, can result in a $1.2^\circ K$ increase in surface temperature. Identical increases in both base and top or elevation, however, result in only a $0.6^\circ K$ in surface temperature.

*Although we have used cloud base height and cloud base altitude interchangeably throughout this report, the two quantities do differ slightly. The height of a point, e.g. the base or top of a cloud, is the vertical distance from the point of observation to the level of that point. The altitude of a point is the vertical distance measured from mean sea level to the level of that point[25]. For our work, the differences are not important.

1.2.1 Definition of Cloud Base

The definition of cloud base is highly dependent upon the technique used to measure it. Current methods for cloud height measurement include the automatic rotating beam ceilometer (RBC), the automatic fixed beam ceilometer (FBC), ceiling balloons, ceiling lights, in-situ aircraft observations and of course lidar [11]. The instrument of choice for routine determination of cloud base height and cover has been the ceilometer. Ceilometers require a bistatic configuration. The rotating beam ceilometer (RBC) consists of a transmitter which is a vertically rotating modulated lamp projection system and a receiver located below the cloud of interest at a prescribed baseline distance from the transmitter. The return is recorded as function of the transmitter's angular displacement. Upon the transmitter beam's intersection with the cloud base and the receiver's field of view, a maximum return is observed. A base altitude may then be determined by triangulation. This is the convention currently in use by the U.S. National Weather Service.

RBC returns have been shown to be greatly affected by cloud geometry and in-cloud multiple scatter in comparison to lidar techniques. The less accurate but more compact and inexpensive fixed beam ceilometers (FBCs) reverse the configuration by having the transmitter fixed at the cloud base and scanning the receiver along the beam path, once lateral alignment has been performed. FBCs offer a low cost supplementary cloud base height retrieval technique to RBCs but are of comparatively lower precision. RBC's tend to indicate higher base heights than lidars and aircraft pilot reports. The recent advent of low power, highly automated, eye-safe laser ceilometer represent a cost-effective compromise between RBC's and more expensive, research lidar systems. Due to the low energies of the commercial laser ceilometers, they have lower SNR, poorer spatial resolution and more limited range.

Algorithms have been developed to estimate cloud base heights from the LANDSAT Multispectral scanner satellite radiance measurements. Although such a platform would have the advantage of global coverage, this technique relies on the shadow cast by the cloud and is thus restricted to certain types of small broken cumulus clouds in specific orientations to the solar angle. As such this technique is necessarily only an estimation for a small set of clouds types in highly idealized conditions. [27]

Lidars specify cloud base by either the altitude where the rapid increase in backscatter signal begins (cloud bottom altitude, r_b) or the altitude at which the backscatter signal reaches its maximum (peak, r_p). The peak signal will always

be located above the cloud bottom. The difference between the two altitudes is dependent upon the scattering properties and hence the microphysics of the cloud in question. This difference can be substantial in some cases but generally becomes less significant as the altitude of the clouds dealt with increase.

The choice of which definition to use for “cloud base” is somewhat dependent upon where the information will be employed. Aviation visibility applications for example may favor the bottom signal location and where cloud opacity begins whereas for GCM implementation cloud extent is critical and the peak cloud signal location may be better. We will present further considerations and discussions for selecting between these definitions later in this report.

Lidar systems allow for measurements of cloud positions with unparalleled precision and improved accuracy [28][29]. Other cloud macroscopic parameters such as cloud top and consequently cloud thickness can also be obtained from lidar profiles. However, this precision can contribute to some of the difficulties involved in deriving cloud altitude information. The complex structure of clouds are highly resolved by lidar. This leads to signatures with multiple peaks and high variances in even single cloud layers. As discussed, multiple scattering effects also add to the ambiguity in the measurement cloud position. In contrast, RBC’s yield rather low-featured, smooth profiles from which cloud base altitudes are easily distinguished, albeit with comparatively limited resolution and range.

1.2.2 The Cloud Base Height Algorithm

Although it is possible to obtain cloud altitude information from direct assessment of individual lidar signatures, evaluating large data sets required automation of this process. Subsequently, an algorithm, developed by members of the ISTS-York University Lidar group, to extract such information [30], has been made use of here to a great extent in this study. It is one of two algorithms used in the ECLIPS International effort to extract such information.

The algorithm utilizes the zero-crossing or sign change of the first derivative of the lidar return signal power dP/dR to identify the rapid increase in return signal which results from the larger cloud droplets present in the cloud. Many such crossings occur in practice resulting from inhomogeneities in cloud structures, as well as from signal noise. It is therefore necessary to develop a set of criteria, to filter out such spurious results.

dP/dr is determined from a least squares fit of a sliding window of successive points from the start to end of the profile. A 3 to 5 point fit has been determined

to be suitable for our data. By combining higher resolution in the range with a larger number of points for the least squares fit, better smoothing of the dP/dr curve and a minimization of spurious zero-crossings, resulting from noise, may be obtained. It is noted, that for lidar signatures containing sharp changes in curvature, an upward or downward bias, depending on the sign of the curvature, in the altitude of the zero-crossing is introduced.

A noise level is calculated corresponding to the return signal at each cloud base (r_b) and a peak altitude (r_p) identified. Zero-crossings where the difference between the return at the base and adjacent peak is less than twice the noise calculated at the peak altitude are regarded as insignificant and rejected. This criteria is also *scale-able* using a multiplicative factor (*corr fak*) and is dependent on the system data acquisition characteristics (ie. detector and electronic line noise) and contributions from optical modifications of the backscatter received by the detectors (ie. *ND* or neutral density filters).

The current rejection criteria for peak signals is given by the expression:

$$P(r_{base}) - P(r_{peak}) \leq corr\ fak \times \sqrt{P(r_{peak})} \sqrt{87 \times range\ resolution \times 10^{ND} \times 1.16}$$

The constants in this rejection criteria formula were calculated for the ISTS Nd:Yag Lidar system in Toronto, Canada. The technical details required for an identical calculation to be performed on the RIVM system are unavailable at this time. We have however obtained satisfactory results with the highest possible sensitivity (*corr fak*) setting (0).

Apart from lidar and in-situ aircraft observations, existing ground-based cloud monitoring systems are incapable of measuring cloud top altitudes. It is possible in all cases for lidar to extract an *apparent* cloud top altitude when the signal falls into the noise. If optical attenuation is not too high the lidar pulse penetrates the cloud completely and the signal transition from the cloud top to the clear air identifies the true cloud top height.

The cloud top altitude, r_t , is defined in the algorithm as the point just below which the return from the cloud decays to the value less than or equal to the backscatter signal at the cloud base. For cases where no measurable clear air backscatter exists at the base, the cloud top is located where the signal drops to the same background intensity as below the cloud. Where the sub-cloud backscatter is well defined, the top is retrieved with improved accuracy by comparing the range-corrected signals.

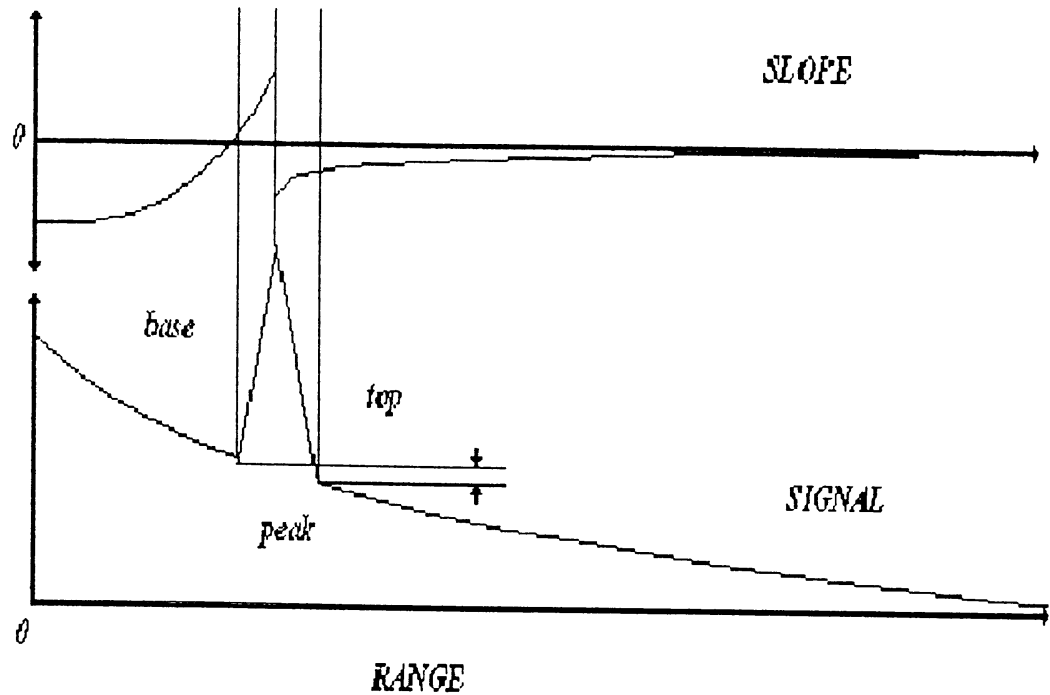


Figure 1.3: Schematic of cloud base algorithm

$$r_t^2 P(r_t) \leq r_b^2 P(r_b) \quad (1.19)$$

The algorithm is capable of locating cloud parameters for multi-layer structures. In such a case, it is given that a region of clear air must exist between adjacent layers. For each r_b value, corresponding r_t values which drop to the clear air value are located. All other peak returns between each base-top pair are ignored. The procedure is repeated for all layers.

Fig. 1.3 is a schematic of the cloud base algorithm.

Horizontal extent of the clouds can be determined using the cloud base algorithm at varying sensitivities to optimize location of the peak returns as a function of time.

1.3 Data Averaging Techniques

The complexity and high sensitivity of lidar systems make their detection components prone to spurious contributions from a number of sources including dark current and background noise. Clouds persistent in time properties allow for an increase in the SNR proportional to the square root of the independent number of samples averaged.

The practice of averaging lidar profiles came with the inception of the earliest lidar systems. The higher the resolution of a system the fewer the photon events one can expect to be detected per trace. Noise becomes a significant contribution, specifically in higher altitudes where photon counts are typically low. The averaging of lidar returns requires that such measurements must be made within rapid succession, such that the atmospheric conditions have not varied substantially within the elapsed interval between such measurements. This requires that the backscattering characteristics be on the same order of magnitude as other sources of noise [31][32]. Essentially, averaging extends the effective “*exposure time*” of the detectors, but without the degradation of pulse length and hence resolution and problems of saturation.

Furthermore, for the most part, clouds are extremely inhomogeneous. Single lidar profiles of clouds alone are rarely representative of the cloud as a whole and as such are not very informative. For studies of radiative transfer, meaningful characteristics from inhomogeneous clouds are often only apparent from data that has undergone substantial averaging processes.

However, within a lidar time series, clouds often move vertically as well as horizontally, across the field of view. Since clouds are inhomogeneous, simply averaging the data over range intervals as previously described inevitably leads to mixing or contamination of the cloud portions of the signal with non-cloud regions. If this were done the cloud’s opacity would be diluted by the “averaging in” of clear atmosphere. This would lead to an underestimation of the clouds actual optical depth. Conversely averaging cloudy regions with clear or non-cloud portions of the profile would lead to an overestimation of the clear atmosphere’s optical extinction. Hence the averaging of subsequent lidar profiles in time must be approached with attention to not compromising the optical characteristics of either the cloud or background atmosphere.

It is also possible to average lidar signals with respect to range. That is, to attempt to minimize the effects of noise by summing and averaging consecutive points along the lidar range resolved profile. This degrades the vertical resolution

of the measurements involved, and again care must be taken not to compromise the cloud optical presence. However, given a sufficient vertical range, and avoiding the cloud portions of the trace, this can be quite an effective treatment to noisy background signals especially in the higher ranges where the SNR is low.

Chapter 2

Inverting Real Lidar Returns: Practical Considerations and Caveats

2.1 Data Quality

Figure 2.1 * shows the expected lidar signal return at $1064nm$ calculated by assuming a pure Rayleigh atmosphere as an attenuating and backscattering medium, calibrated and plotted with the data from a cloudless sky on August 4th, 1993 from the RIVM lidar system. This calibration in effect serves to provide our theoretical lidar signal with the constants at the front of the lidar equation, Eq. 1.1.

We note that the actual return is less than optimal beyond a range of approximately $1200m$. This shortfall can be attributed to a number of factors not taken into consideration in the calculation of the signal.

By far the most important factor that has not been included in this projection is the presence of atmospheric aerosols in the boundary layer. From the authors experience, these typically have optical extinction values on the order of $10^{-2} \frac{1}{km}$. This strong attenuating presence is a possible explanation for much of the losses

*Many of the following figures in this section have been produced from data processed by the the software package KNMI2B2 developed for this project and to be described in the next chapter.

The package uses the algorithms and techniques previously described for and analyzing cloud lidar data. The software package Origin by MicroCal Software Inc. a Windows 3.0 application has been used to present the data here. Please consult the documentation that accompanies Origin and MicroCal for more details.

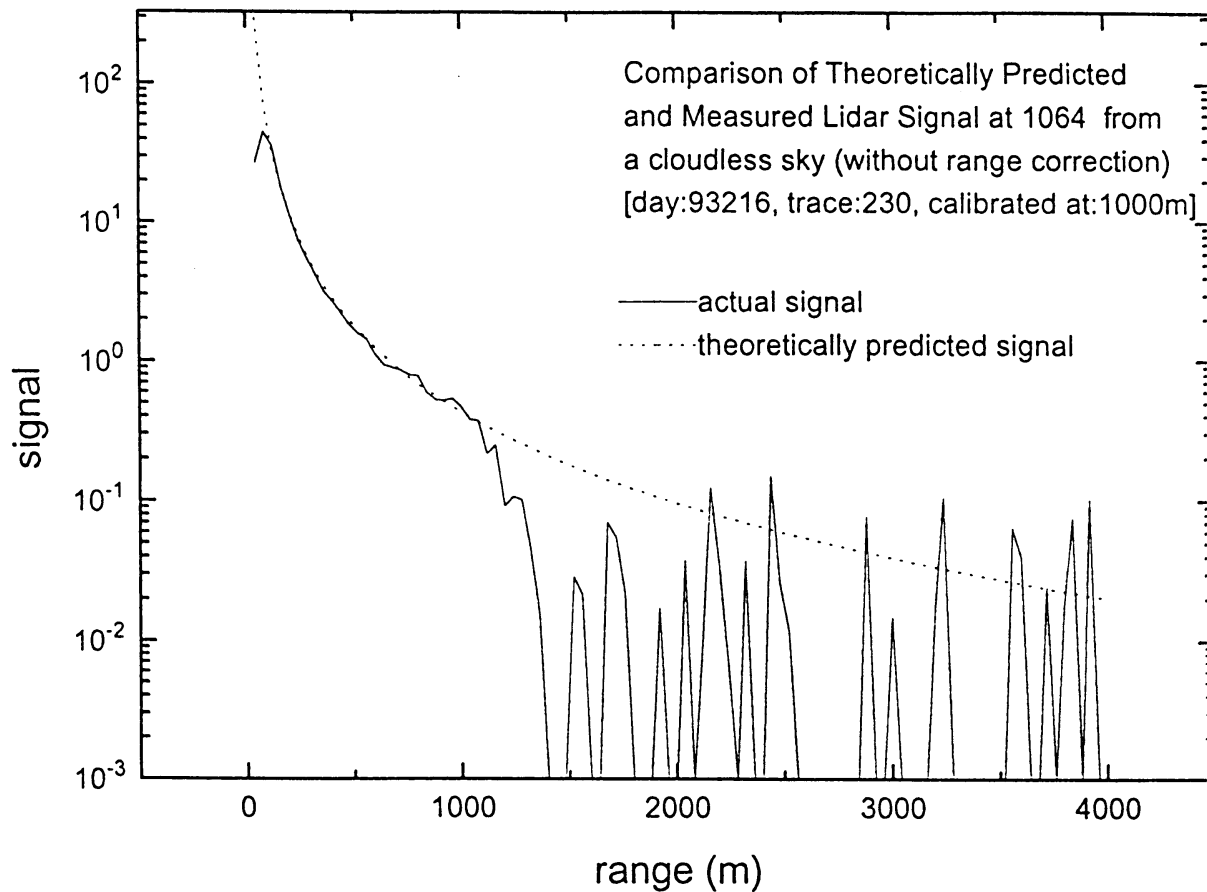


Figure 2.1: expected lidar signal return at 1064nm calculated by assuming a pure Rayleigh atmosphere as a attenuating and backscattering medium, calibrated and plotted with the data from a cloudless sky on August 4th, 1993 from the RIVM lidar system

early in the profile leading to this rather modest range depth for the system.

As the system is an *aerosol boundary layer* lidar, the optics, transmitter and receiver have not been *optimized* for clouds. The amount of adjustment required to recently realign a similar RIVM system for clouds can attest to the marked difference between the two configurations [22]. Furthermore, any digitizing system has inherent limits in its ability to resolve low signal levels, and this is clearly the case for regions beyond 1200m.

Complicating the issue further is the presence of *after-pulsing* or *ringing* in the detectors when exposed to high signals. Figure 2.2 shows two individual backscatter profiles (74 and 225) taken from the same day, August 4th, 1993 [Julian date:93216].

Profile 74 clearly represents a saturated cloud return, with a signal value maximum of about 32000. Note that although this maximum value is located far beyond the height we expect to detect any signal from the background atmosphere there appears to be some signal above the cloud which is higher than the signal of the background atmosphere prior to entry into the cloud.

Compare this to profile 225, with a much lower cloud peak signal (6000) which is clearly not saturated and is located below 1500m, within what we expect to be the range at which the background atmosphere will be detectable by the system. The signal above it clearly is lower than the signal prior to entry into the cloud. This is the result of attenuation of the incident and return pulse by the intervening medium, specifically the cloud, as we expect.

While it is possible that there is a strongly backscattering aerosol or haze layer above the cloud in trace 74, more than likely what is being observed are the effects of after pulsing or ringing from the photodetectors in question, avalanche photodiodes (APD). This is quite a common problem with such detectors[33]. It was initially expected at the start of this study, by the technical personnel primarily involved with the system, that the recovery time of the detectors was smaller than the time resolution of the data acquisition components. Recently it has however been confirmed that this is not the case and that we are observing after-pulsing in our recorded data[22].

The accuracy of the Klett inversion is dependent upon the accuracy of the boundary condition, the reference optical extinction. As was previously discussed, unless it is otherwise known, the application of the inversion requires an estimate. The reference height is selected above the cloud, with the expectation that the only optically scattering or attenuating constituent at that height will be atmospheric molecules. If a sonde measurement is taken providing the

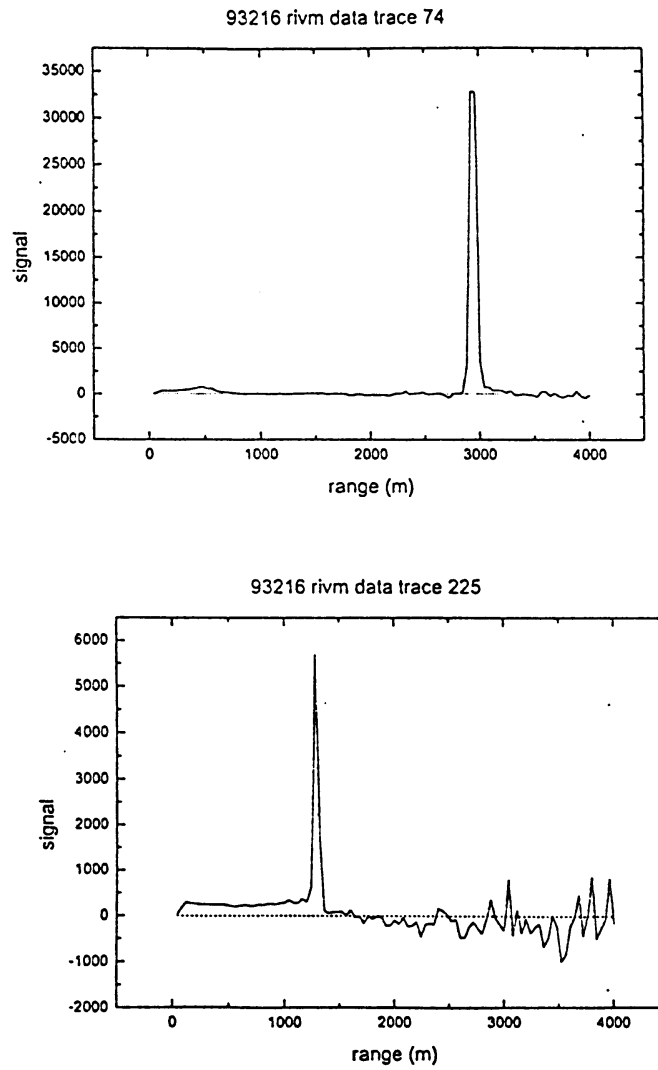


Figure 2.2: Lidar backscatter profiles from August 4th, 1993 [93216], trace 74 (*top*) and trace 225 (*bottom*).

Table 2.1: Technical Overview of the RIVM Truck Mounted Nd:YAG 1064 nm, 70 mJ Aerosol Boundary Layer Lidar System

Transmitter	
Wavelength	1064 nm
Pulse repetition	10 Hz
Pulse length	9 ns
Pulse energy (simultaneous output)	70 mJ at 1064 nm
Beam divergence	1 mrad full angle
Receiver	
Telescope field of view (FOV)	32 cm (diameter) Fresnel lens 3.1 mrad full angle
System FOV	0.5 mrad
Optics	2% transmission neutral density
Detectors	APD at 1064 nm
Signal processing	transient recorder
Data acquisition	
transient digitizer sample $f = 100 \text{ MHz}$ averaging: 250 shots/25 sec. every 4 minutes; 24 hours/day other: background subtraction using pretrigger pretrigger length: 5ms (500 analog data points) data: range (index) corrected, scaling factor (unknown)	

pressure and temperature at or near that height, the optical extinction can be calculated and used as our boundary condition.

However, if after-pulsing occurs, the signal values above the cloud are then not the result of backscattering from a molecular atmosphere, but an artifact created by the detection system. Hence, it is advised that a reference height be chosen sufficiently high enough above the cloud that one is confident that the inversion starts with values that are backscatter and not after-pulsing. Furthermore, near saturated data should be approached with caution and of course, saturated data discarded.

In Table 2.1 are some technical details relevant to our work regarding the lidar system under question.

2.2 Practical Application of the Klett Inversion Algorithm

In our work only a basic rectangular numerical integration was performed. As we are dealing with relatively large data sets, previous studies have shown that a more sophisticated routine does little to improve our results [3]. Furthermore, since we have derived this solution from Eq. 1.1, as we have discussed in Sec. 2.1.5 such an inversion will not account for multiple scattering effects. Monte-Carlo simulations indicate this deficiency can only account for a contribution on the order of 10 percent. In fact, for clouds of low optical depths, such as most cirrus, multiple scattering contributions can be negligible [16] In general C and k in Eq. 1.7 can be range dependent however it has been found that good inversions can be obtained by using constant values for these quantities. We discuss the potential for taking into account a variable backscatter to extinction ratio instead of C in the final section of this report.

In general, k has been set to unity, and it has been accepted that there are no *stringent* reasons for any other choice. It has also been reported that extinction inversions such as *Klett's*, depend only weakly on k . [34] In most cases, both the constant of proportionality and k are taken as constant along the path of inversion. Mulders [35], has found them to vary greatly in the same temporal and spatial fields. Studies of the sensitivity of Klett's inversion to the parameters have shown small variations in k to have little effect, except in cases where $\sigma(r)$ is at or near singularity [36]. Varying k to suit the expected cloud can be difficult and sometimes impossible to determine for real atmospheric conditions. Past efforts, using varying k values have shown very minor improvements while involving a major increase in computational time. [3]

2.2.1 Estimations of the Reference Altitude and Extinction

For the far-end inversions, the reference altitude for σ_f is chosen as high as possible, as long as there is a good SNR. In doing so, errors incurred by inaccuracies in the σ_f value decay to a reasonable level before approaching the lower altitude region of primary interest.

The reference height is chosen high enough to be relatively safe in assuming that backscatter from this altitude was predominantly from a molecular or a Rayleigh atmosphere. Figure 2.3 is a plot showing a optical extinction profiles

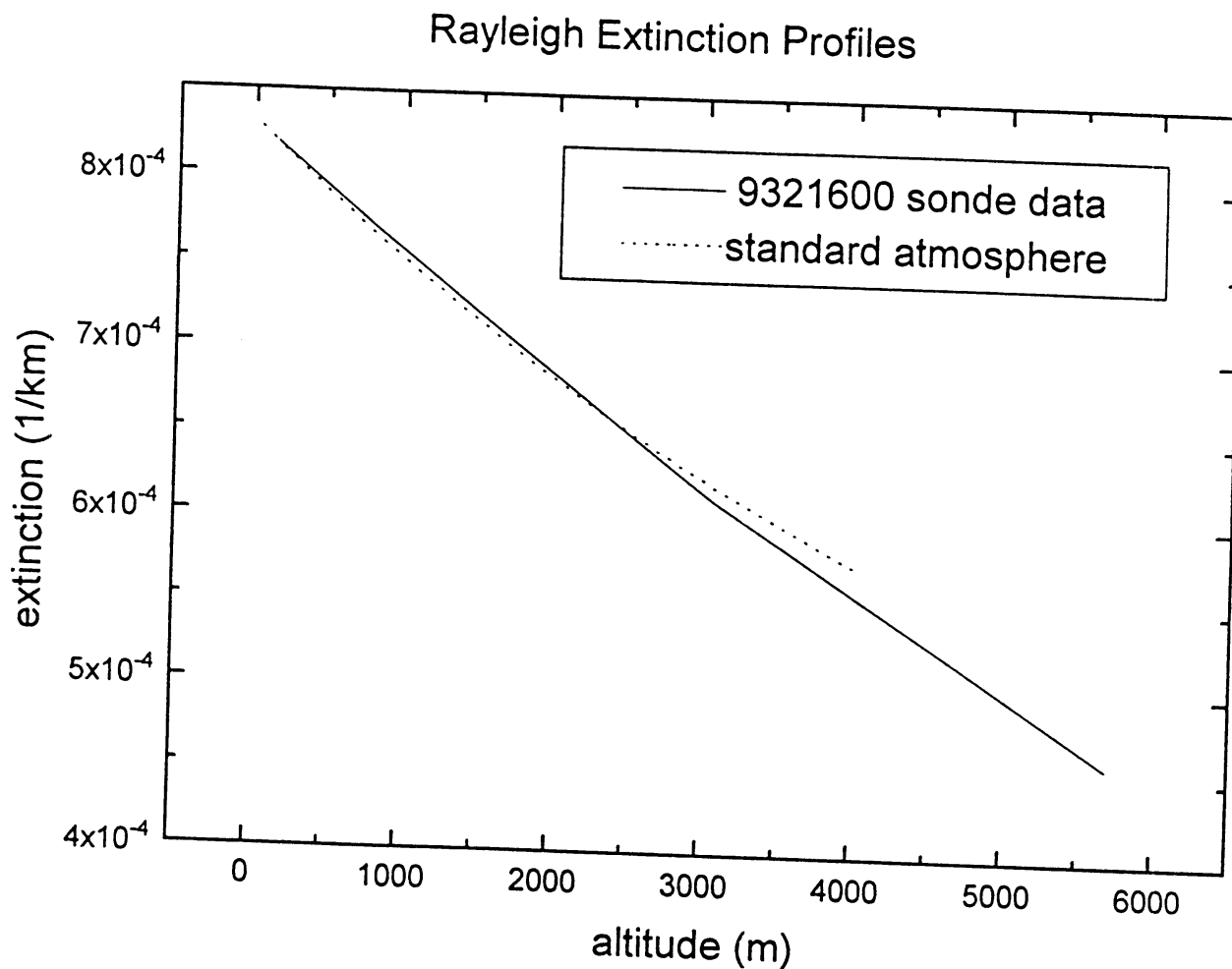


Figure 2.3: Graph showing optical extinction profiles for a pure molecular or Rayleigh atmosphere at $1064nm$. Generated using sonde measurements (—) and using an assumed lapse rate of $-6.5^{\circ}C/km$ and the hydrostatic pressure equation (---)

for a pure molecular or Rayleigh atmosphere at the $1064nm$. wavelength. We have generated one profile using an assumed lapse rate of $-6.75^{\circ}C/km$ and the hydrostatic pressure equation.

It should be noted that backscatter contributions from molecular as well as aerosol atmospheric constituents are relatively low at the $1064nm$ wavelength, hence we would expect very low SNR as such. This results in difficulties in specifying reference values for Klett Inversion as we will discuss in length. This low backscatter is the result of a rather small cross-section at in the infra-red region. At $1064nm$, this translates into an area of $10^{-32}m^2$, approximately one order of magnitude less than in the visible at $532nm$. One can conclude immediately, that such a consideration would indicate that a visible wavelength would be preferable for optical measurements using lidar, and as well will show, this is largely the case.

Based on the assumption that aerosol and molecular components are the only constituents at a chosen reference altitude a reference extinction value can be calculated using a molecular atmosphere. The Rayleigh calculations can utilize meteorological parameters obtained from sonde measurements.

The success and failure of the Klett Inversion depends on a number of factors, however Klett [21] identifies the most critical as being the selection of an accurate as possible reference value for the extinction (*boundary value*).

From the work performed on the RIVM data set, we have found that proper selection of a reference signal value and reference height are also important considerations.

Figure 2.4-2.5 shows a simulated relative range-corrected logarithmic lidar backscatter signal for a simulated *plateau shaped* optical extinction profile and an Klett inversions of the backscatter using varying values for the reference optical extinction boundary condition, respectively. This is similar to the simulation performed in Kletts original article describing this technique[21].

From Figure 2.5, it is apparent that the inversion is quite *forgiving*, with respect to uncertainty in the estimation of the reference optical extinction boundary condition, σ_f . The correct value σ_f is $\frac{1}{km}$, however, estimations as high as 100% above and 50% below the correct value still result in a convergence to the correct profile.

Figure 2.6 is a similar result but for the case of a simulated constant extinction profile, from which it is easier to gauge the effects of errors in our boundary condition estimate of σ_f . It can be seen that the inversion has corrected itself to within 10% of the actual value regardless of high above or below we have

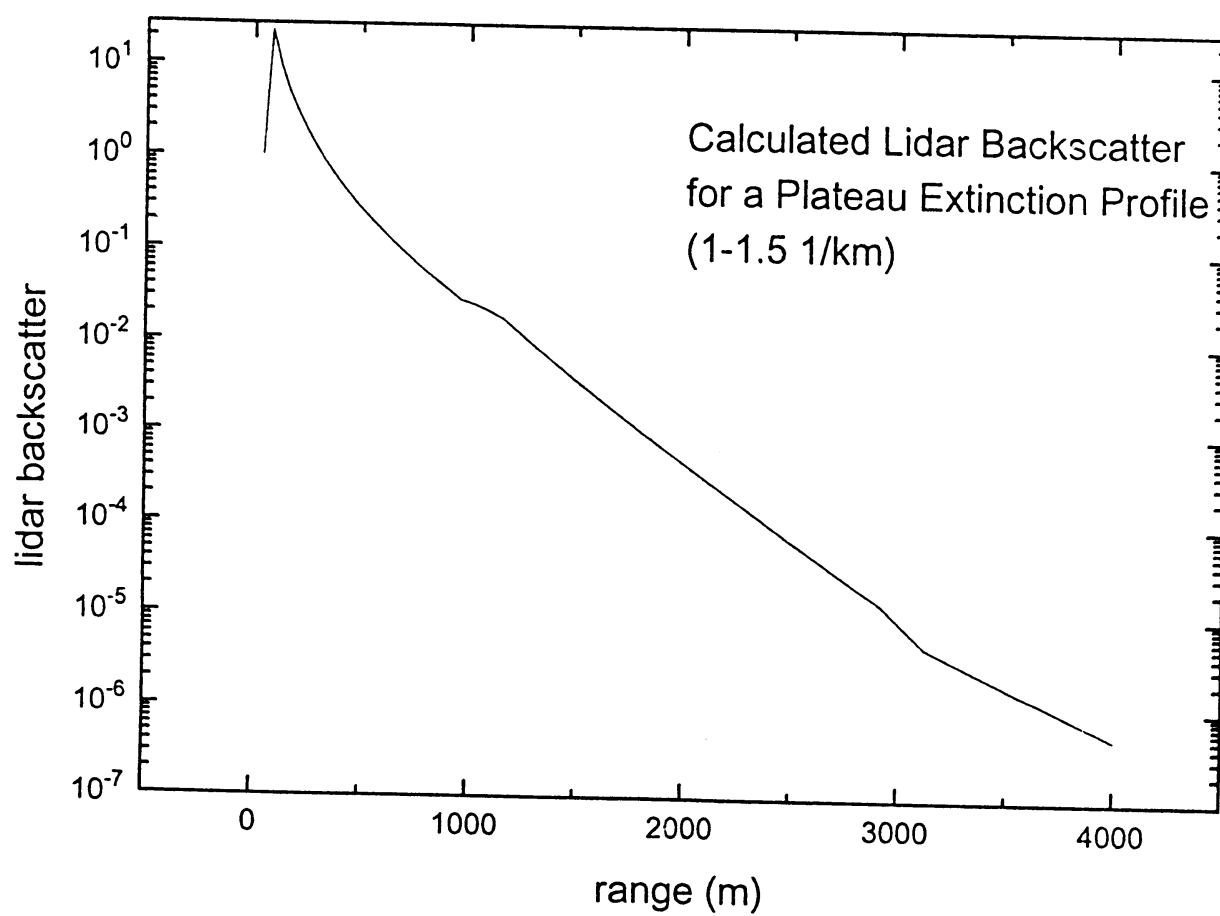


Figure 2.4: Simulated relative range-corrected logarithmic lidar backscatter signal ($S - S_0$) for a simulated *plateau shaped* optical extinction profile

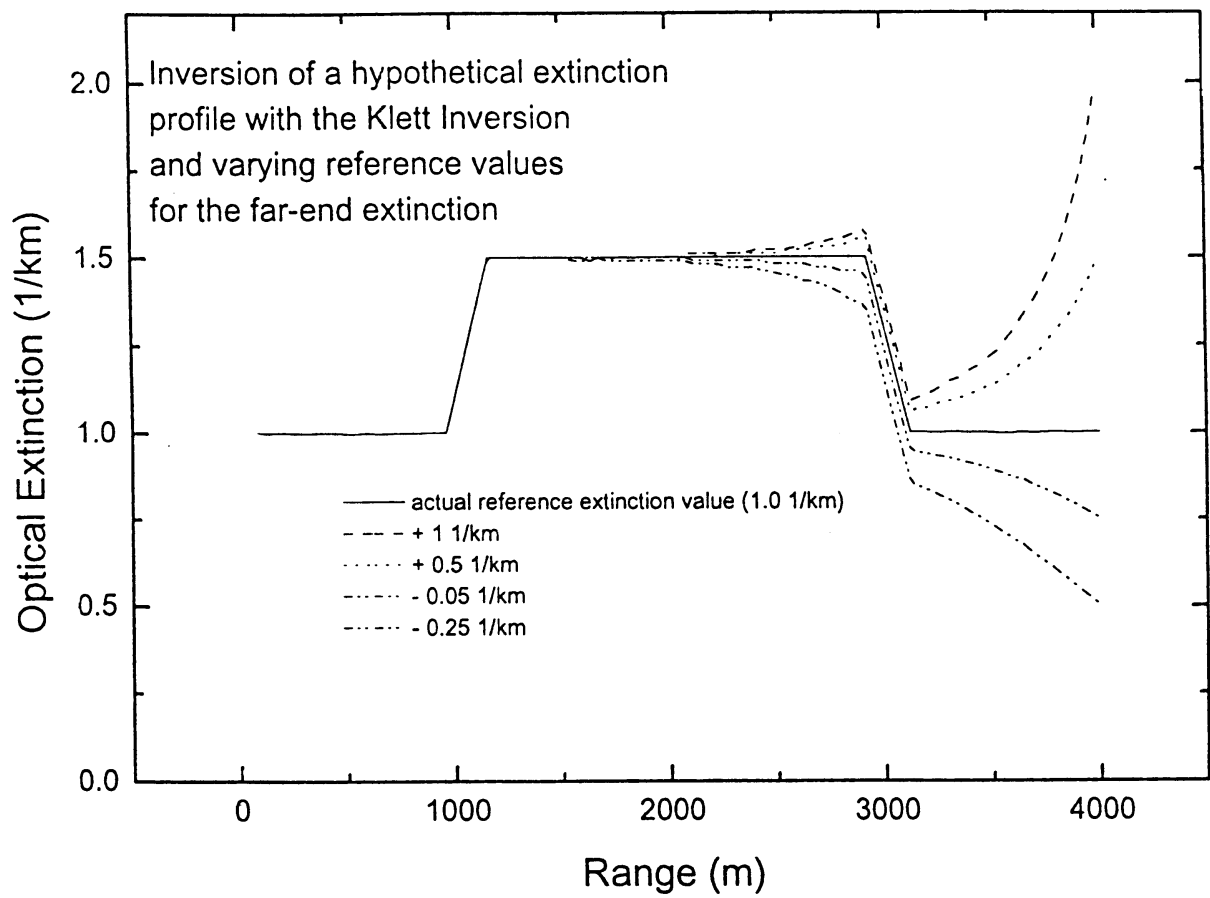


Figure 2.5: Klett inversions of the previous simulated backscatter profile figure using varying values for the reference optical extinction boundary condition, σ_f .

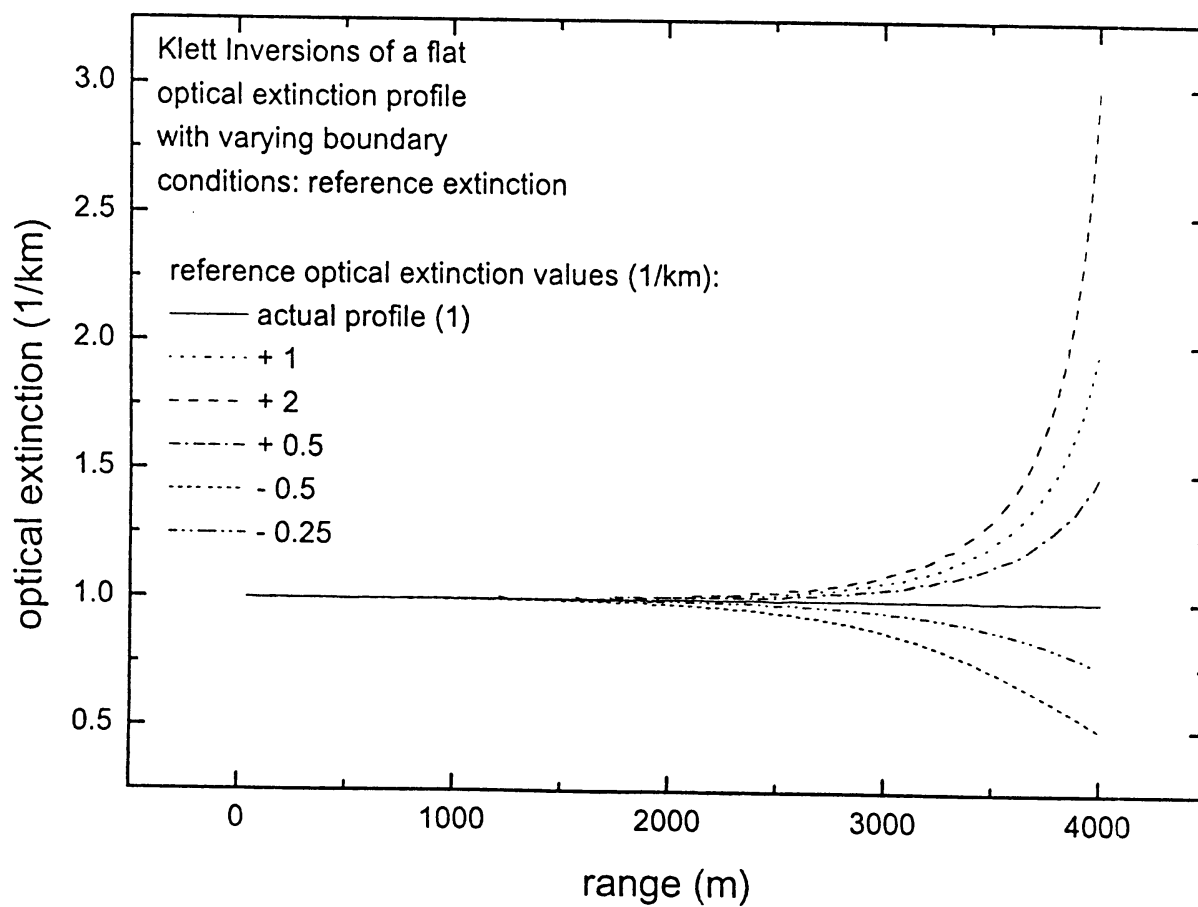


Figure 2.6: Klett inversion of a simulated constant extinction profile using varying values of σ_f .

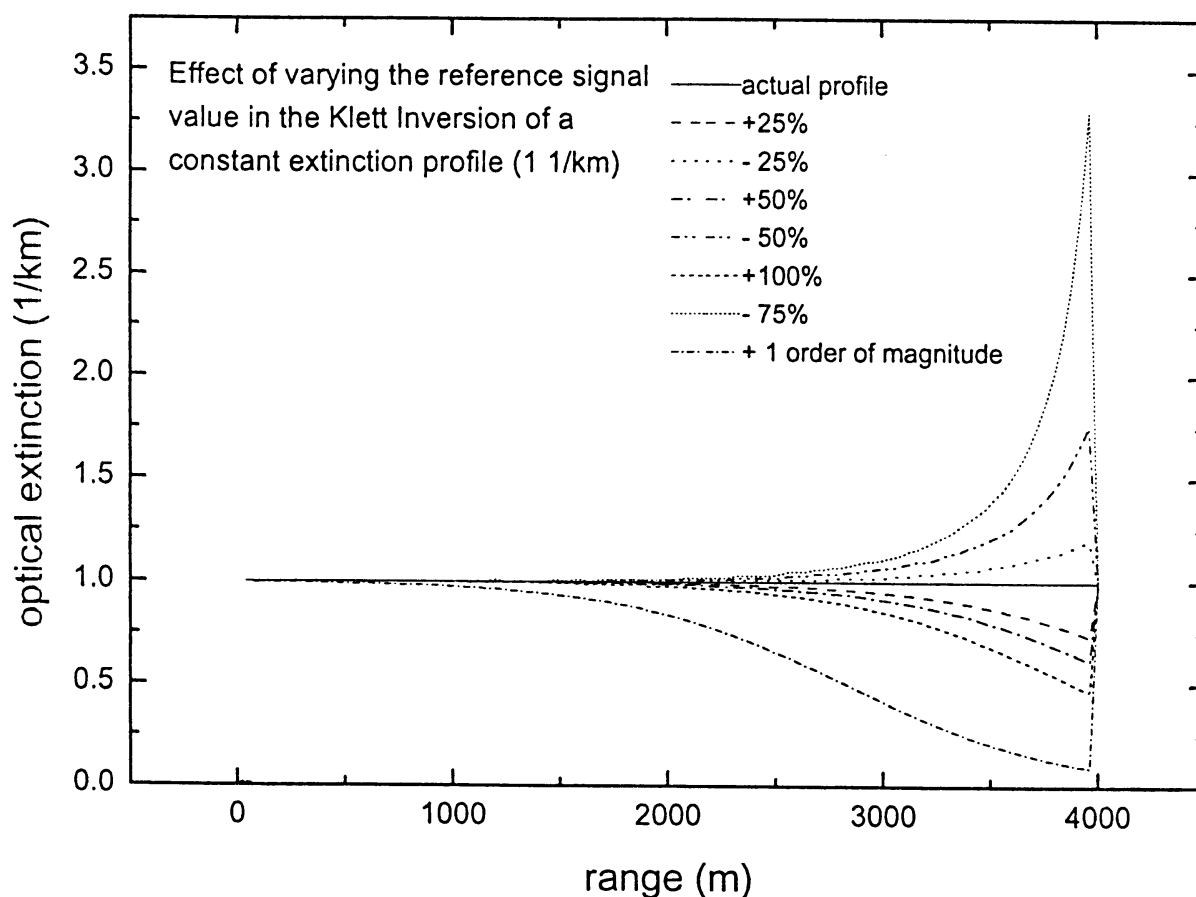


Figure 2.7: Klett inversion of a simulated constant extinction profile using varying values of reference height signals.

estimated σ_f from the correct value. However it should be noted that errors in the inversion which result from an underestimation of σ_f tend to propagate further down the length of the profile and are hence more detrimental.

Similar analyses have been performed for errors in the reference height signal value and addition and subtraction of constant values to the entire profile and are shown in Figures 2.7-2.8, respectively.

As previously, discussed, we choose our reference height at which we start our inversion as high as possible. Since the detected atmospheric backscatter at high altitudes from the system is low or nonexistent, we expect that these reference signal values will most likely be erroneous data which are nothing more

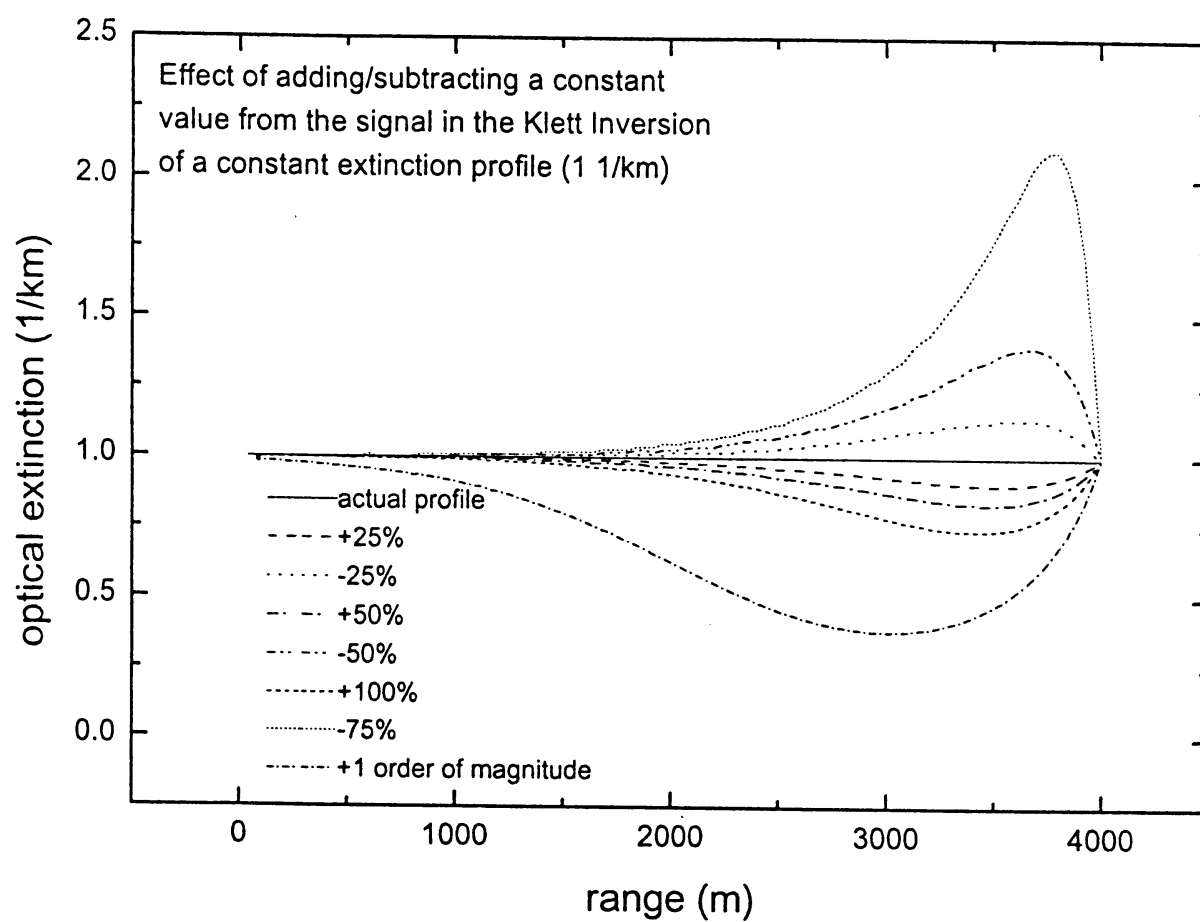


Figure 2.8: Klett inversion of a simulated constant extinction profile with varying constant values added and subtracted to the entire profile.

than pure noise from the detector electronics. Thus an assessment of the effects of an incorrect value in the reference signal must be obtained. From Fig. 2.7, we see values below the actual signal result in initial over prediction in the optical extinction, but which correct themselves rather quickly. For values above the correct signal we see an initial underestimate in the optical extinction which is slow to recover to the correct profile values.

The latter analysis, Fig. 2.8, was performed with an interest in assessing the effects of *background subtraction*. This is a common practice in the processing of experimental lidar data. A value for noise which results from the system data acquisition electronics etc., is obtained from a portion of the digitized signal either before or after the active triggering range in which the atmospheric measurement takes place. This value usually an average of the signal over this pre or post trigger range and is subtracted from the entire profile, so as to obtain a signal profile which is *ideally* the result of only the detected atmospheric backscatter.

For noisy signals this often results in zero-crossings of the backscatter signal values. This is not permitted by our inversion mathematically as we must define the logarithmic-range adjusted power, Eq. 1.8, which will then be undefined for such values. In our case, we know that our signals are quite noisy, specifically beyond the 1200m range, and expect many zero crossings. In such a non-ideal case it is sometimes useful to reconstitute the original backscatter signal by re-adding this background noise value to the profile. If this value is not known or if the data acquisition component records spurious negative values for low SNR regions of the data then it is useful to add some constant to the profile also.

From Fig. 2.8, we observe that subtracting a constant value from the actual signal results in initial over prediction in the optical extinction, but which correct themselves rather quickly. Adding constant values to the correct signal however, results in an initial underestimate in the optical extinction which is slow to recover to the correct profile values.

To gauge the relative contributions of varying all these boundary conditions, Fig. 2.9 shows the range at which the recovery of the inversion to within 10% of the correct value occurs when varying the reference optical extinction value, reference height signal value and a constant is added or subtracted to the profile.

It is seen that the inversion is relatively robust to positive uncertainties in the reference extinction value chosen whereas underestimation of this value tends to have more far reaching effects as we previously mentioned. The algorithm is far more sensitive to errors in reference height signal and to background addition. An underestimation of reference height signal tends to recover faster than

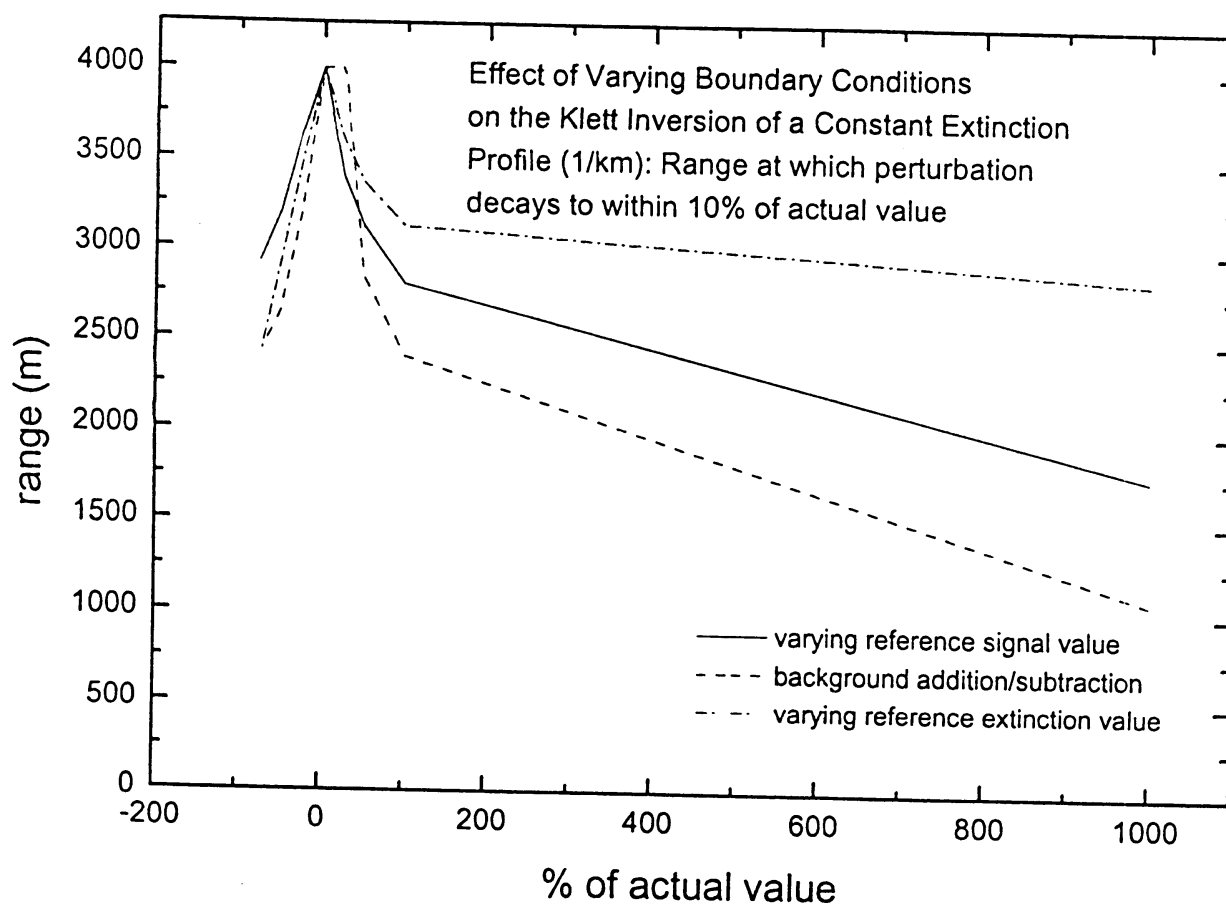


Figure 2.9: Graph of range at which varying the reference optical extinction value, reference height signal value and constant added or subtracted to the profile effect of the height at which the recovery of the inversion to within 10% of the correct value occurs.

an overestimation and background addition or subtraction tends not to affect the inversion provided the constants added or subtracted are sufficiently small (within 100% of the signal value).

Upon reexamination of the inversion algorithm, Eq. 1.13, the reason behind such attributes of the inversion becomes clear. For large positive values ($\sigma_f \rightarrow \infty$) of the boundary condition term, $\frac{1}{\sigma_f}$, in the denominator of Eq. 1.13, the contribution to the algorithm is quite small. As σ_f becomes small however ($\sigma_f \rightarrow 0$), this term becomes much larger in the denominator leading to underestimations of the extinction.

It can also be seen from Eq. 1.13 that the reference height signal given as a logarithmic range adjusted power, S_f , affects the inversion throughout.

The recoverability of the inversion is largely due to the introduction of higher and more accurate values further downstream in the signal which dominate the inversion and bring it towards the correct values through terms such as the integral in the denominator. Although such uncertainties become less and less significant as the inversion proceeds, it is important to note that, again, because of the integral term, noise and other errors in the data have some, if not modest effect throughout. It is there always in our best interest to reduce such effects through averaging or any other method available. It should be noted that the propagative effects of noise are not discussed here but have been covered elsewhere [21].

In general, it is the relationship between the reference height signal, S_f , and the reference extinction coefficient, σ_f , that *calibrates* the inversion of the signal throughout. A grossly inaccurate estimate of both can lead to potentially disastrously inaccurate results, especially for values near the reference height.

2.2.2 Use of Averaging Techniques

The conventional averaging method to improve SNR is with respect to time, as we have previously mentioned. This is not advisable for our data since both clouds are extremely variable in time and our duty cycle of four minutes between data acquisition cycles is too long. Clouds that are seen in one signal trace can completely disappear within the next subsequent profile. Hence averaging such consecutive returns would result in a meaningless profile.

Should our data acquisition protocol change to a more consecutive and continuous procedure this may be possible. This method effectively extends the exposure time of the detectors without degrading resolution and causing saturation.

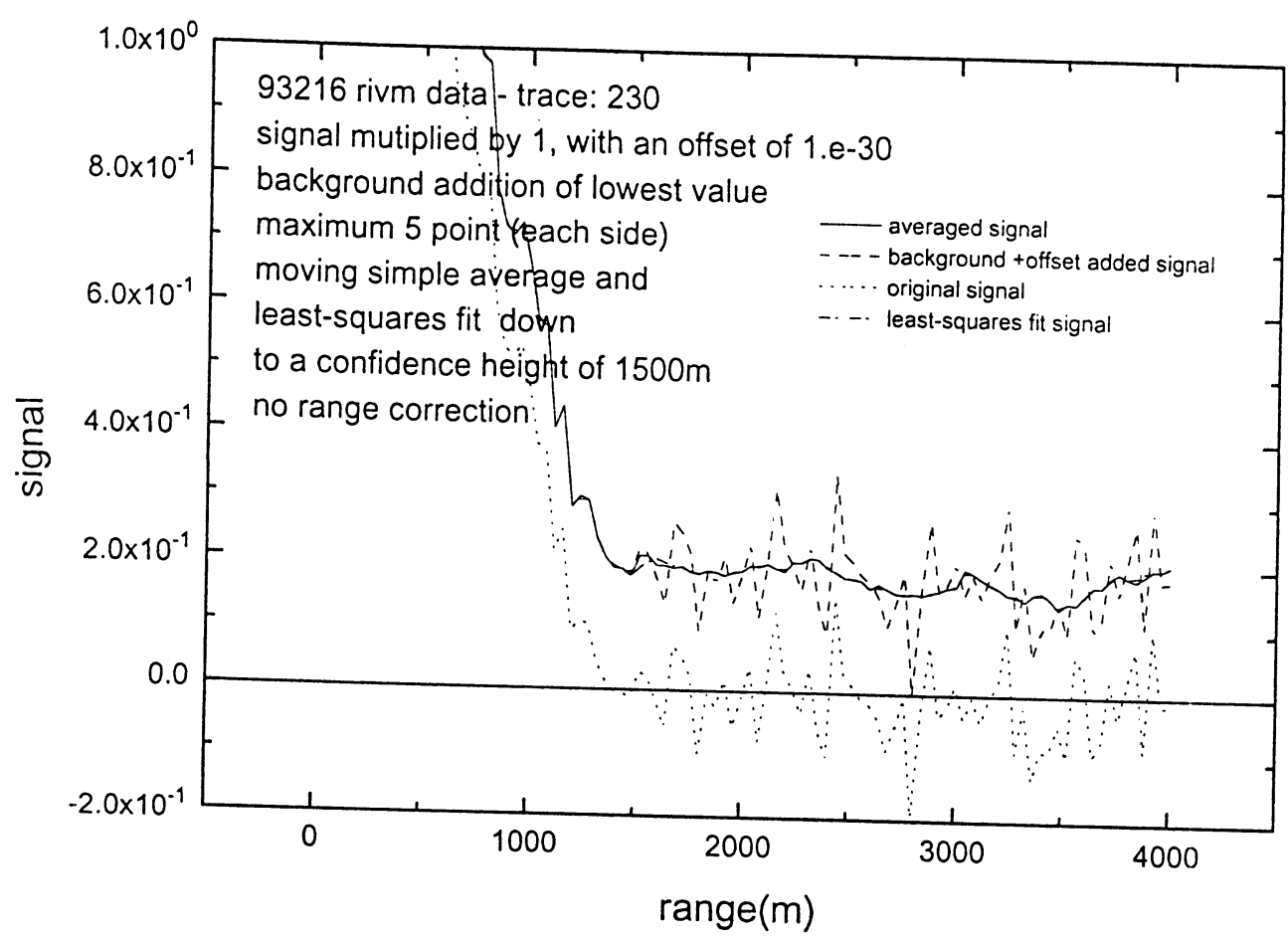


Figure 2.10: Plot of an original lidar backscatter signal as collected from August 4 1993 [93216] ((.....)). A profile where the value of the most negative signal value is added to the entire profile along with a small offset is also plotted ((——)). Signal values from the topmost range height (4000m) down to 1500m (the height at which we expect to begin to detect some of the background atmosphere) are averaged or fitted to 5 points above and below the signal point of interest and shown as ((——)).

There have been some encouraging indications from a similar system at the RIVM recently modified to collect the data at in more continuous duty cycle. Averaged data from this system appears to detect the background atmosphere at ranges of approximately 4000m and suggest that this maybe remedy for the poor detection capabilities of the present system [22].

Figure 2.10 shows the possible techniques that can be used to condition our present lidar backscatter profiles prior to inversion. Here an original signal as collected is plotted. The value of the most negative signal value is added to the entire profile along with a small offset and is also plotted. Finally, signal values from the topmost range height (4000m) down to 1500m (the height at which we expect to begin to detect some of the background atmosphere) are averaged or fitted to 5 points above and below the signal point of interest. Note there is little difference between the fitted and averaged data result. In general it is recommended that the data be averaged and not fitted. As the result is mostly due to supposedly random noise it makes little intuitive sense to *fit* to it.

2.2.3 Example of an Inversion of Real Data

Figure 2.11 is a plot of a range corrected signal (trace 6) from August 4th 1993 [93216]. It shows relatively strong cloud return around 1200m.

Figure 2.12 shows several inversions of that signal using a variety of values for the reference extinction coefficient, with and without averaging. Regardless of the chosen boundary condition or the averaging of the data, the inversion converges to a peak value of about $5 \frac{1}{km}$. Below the cloud layer, from 500m to 1000m we see the boundary layer aerosol contribution, which appears to be approximately $10^{-2} \frac{1}{km}$. Values calculated for ranges higher than 1500m are completely unreliable however.

This cloud optical extinction result below 1500m compares well with values predicted from models calculated by Wright et al., from a modified scattering model of Deirmendjian [37].

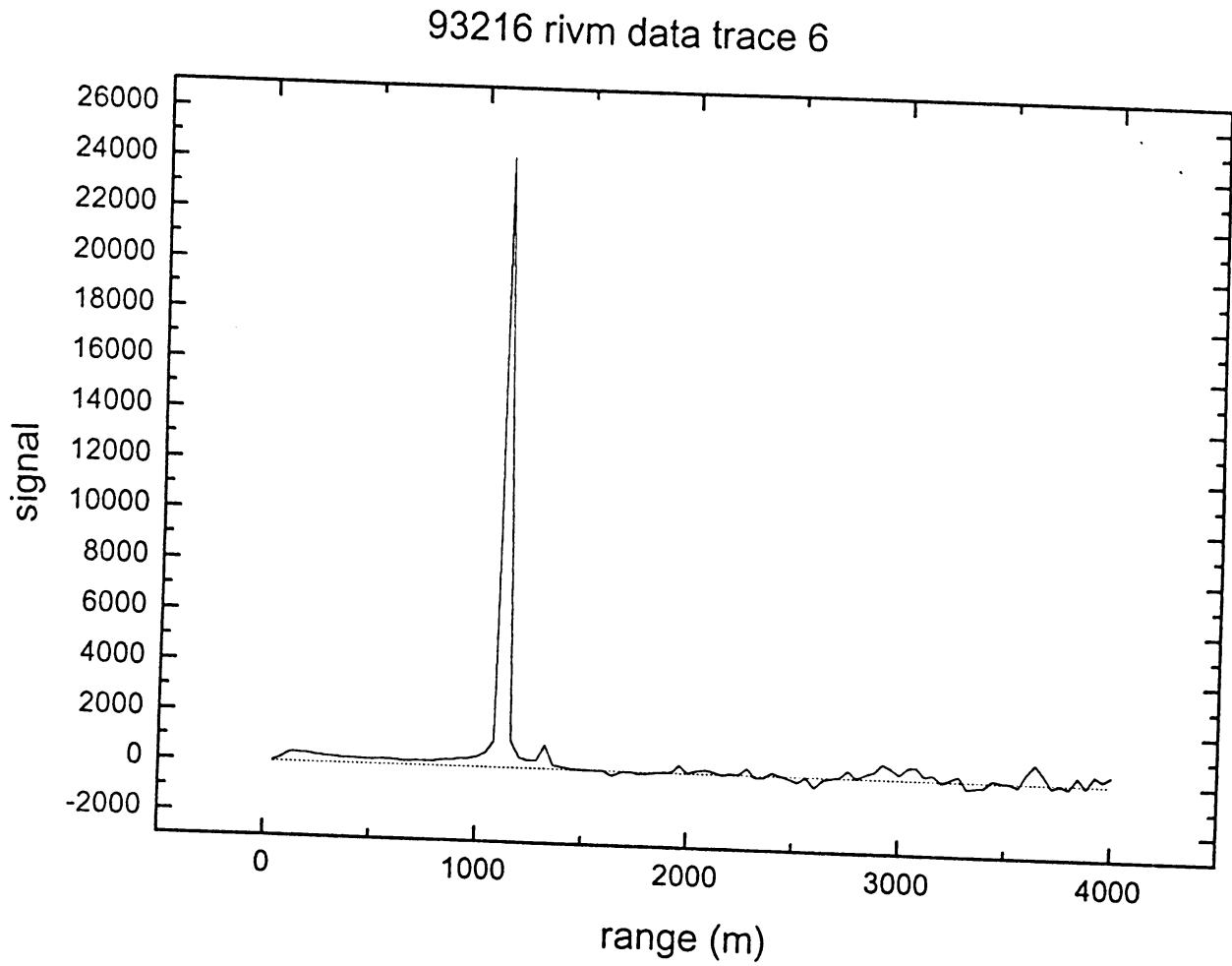


Figure 2.11: Plot of a range corrected signal (trace 6) from August 4th 1993 [93216]

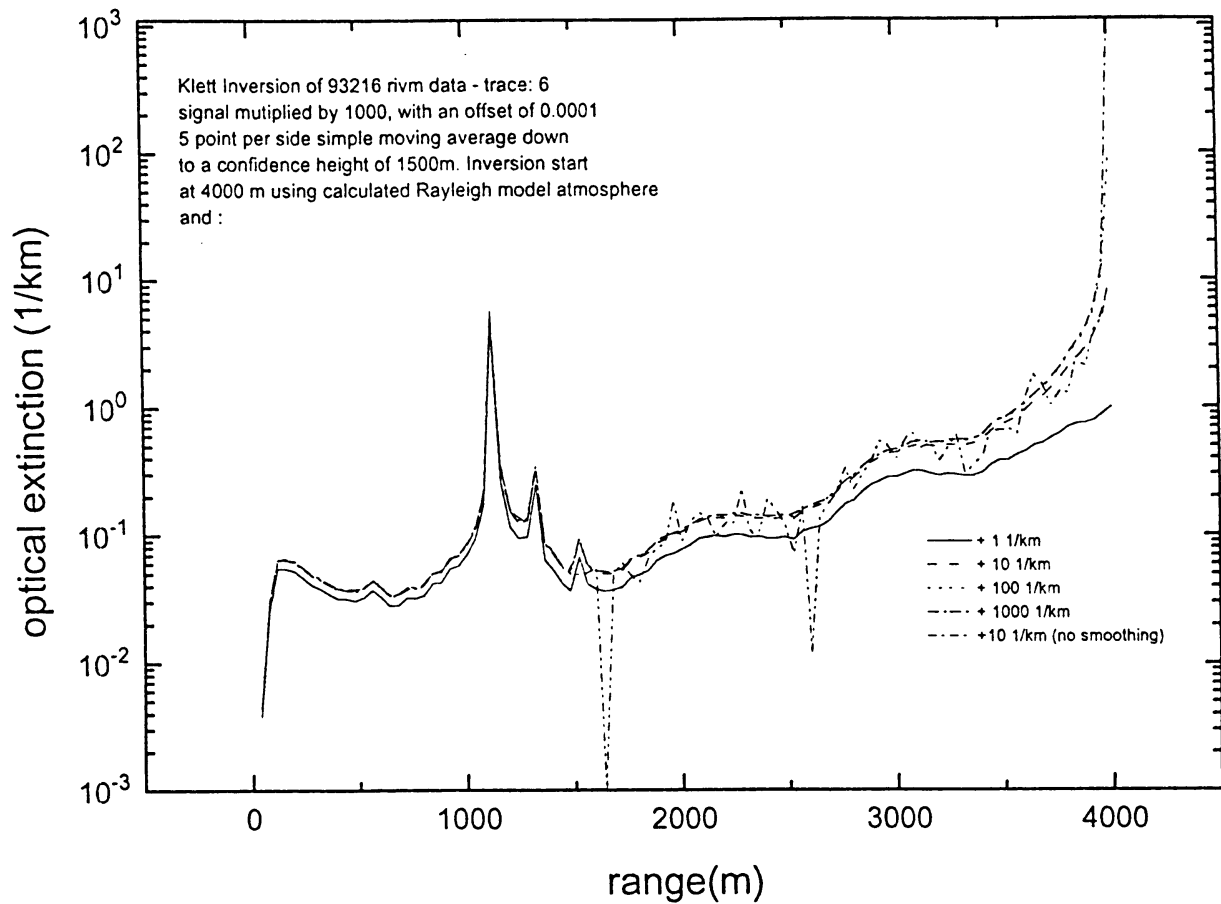


Figure 2.12: Inversions of a signal (trace 6) from August 4th 1993 [93216] using a variety of values for the reference extinction coefficient, with and without averaging.

Chapter 3

KNMI2B2 Main Code General Requirements:

KNMI2B2 was written and designed to operate on any PC Compatible platform. All graphical examples have been generated through the software package Origin by MicroCal Software Inc. in a Windows 3.0 environment. The source code is written in MS-FORTRAN 5.1 and is approximately 1900 lines in length. Currently there are 32 adjustable parameters which will be described in this chapter.

3.0.4 KNMI2B2 Main Code Operating Description:

In our description and instructions we will be using the sample data set 93216riv.dat provided to us by RIVM. This file is formatted with each return profile or trace as a 100 data point row 6 integer digit wide ASCII data separated by single spaces between points. KNMI2B2 reads this data in as real numbers with a width of 7 digits and no decimals. In the past, the data has been range corrected, although the user can specify uncorrected data also, provided the data is similarly formatted. As each trace is read a saturation flag in a time index file is also read. The flag indicates if a signal contains saturated data.

The parameter file known as para.dat which gives the program its operating instructions for performing calculations, the lidar data and knmi2b.lis which assigns filenames to the many program data products are read first. Data such as lidar radiosonde filenames are also read here. The lidar data is read in the format described above. Range correction if required, is removed and an array is created with the logarithmic values of the signal for use in the cloud base algorithm. At this point the user can have specified in the para.dat file to

multiply or sum to all the data by a constant, set all data below a certain set value to that set value and/or smooth the data by averaging or fitting a line from the topmost range height down to any specified height.

Data and parameters are then passed to a subroutine called club which locates the cloud base, peak return signal and apparent top or penetration height index from the array containing either the logarithmic or linear values of the lidar backscatter (depending on the users discretion). For 1064nm a logarithmic signal is preferred. This is a modified version of the ISTS cloud base height algorithm known as icb.for. It is currently limited to locating up to 3 cloud layers [30].

If the data is not saturated then the radiosonde data is read in next. From it, a Rayleigh pure molecular atmosphere is calculated and a value for the boundary condition or reference extinction coefficient is interpolated between the two points bounding the inversion reference height in the sonde data. The reference height can be specified either as some fixed height above all clouds in the time series or at a fixed set height in para.dat. The user can choose from the far-end or Klett, a modified Klett for $k = 1$ described in the previous chapter by the Eq. 1.14, or slope method inversion algorithm to invert the data and obtain an optical extinction profile [21].

A subroutine then calculates the optical depth and mean extinction from this profile. These two data are also calculated by comparing the signal just above and below the cloud, using the *ratio method*. Finally the meteorological parameters read in from the sonde data are correlated with the clouds optical and geometric properties and all of these results written to the previously specified files listed in knmk2b.lis.

If however the saturation flag is positive and the operator chooses to, the previous steps following the cloud base height algorithm can be omitted. All files are then closed and the program terminates.

This is a completely self-contained program. There are no outside objects to link as all the subroutines are attached to the main source code listing, should modifications and a recompilation of the program be required. Below is a flow chart (based on ANSI X3.5-1970) of the program schematic, it will be useful to refer to this when using this package (see Figures 3.1-3.3).

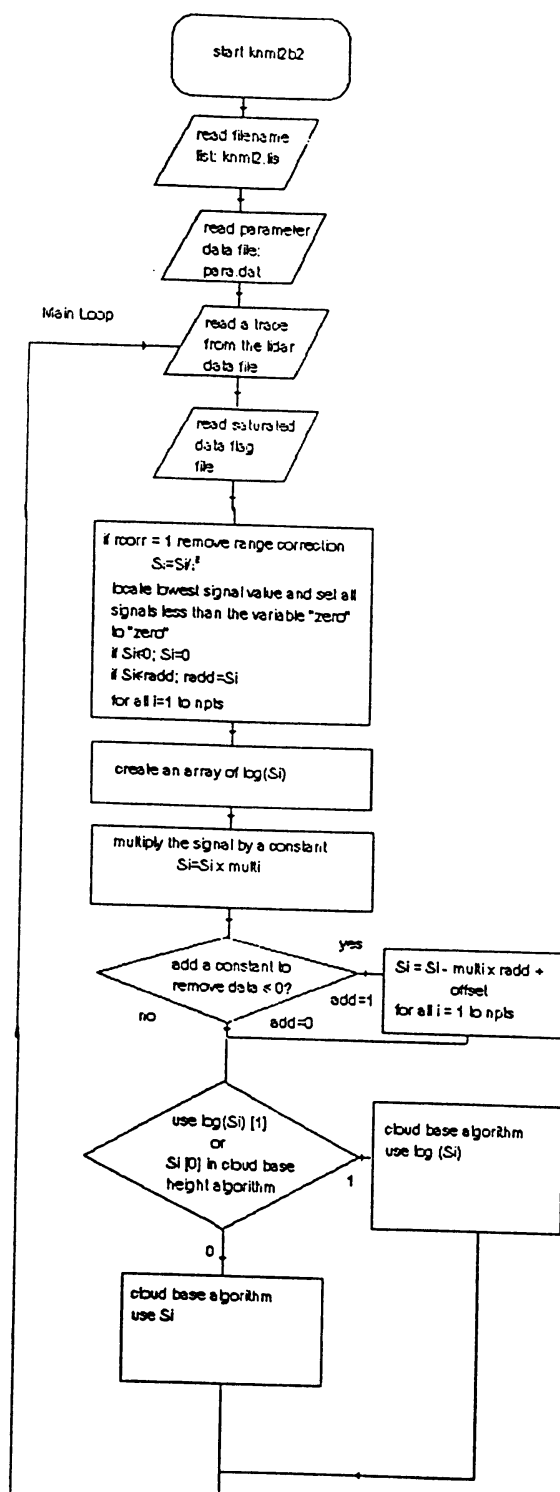


Figure 3.1: Flow chart of the KNMI2B2 software features and data processing scheme, part 1.

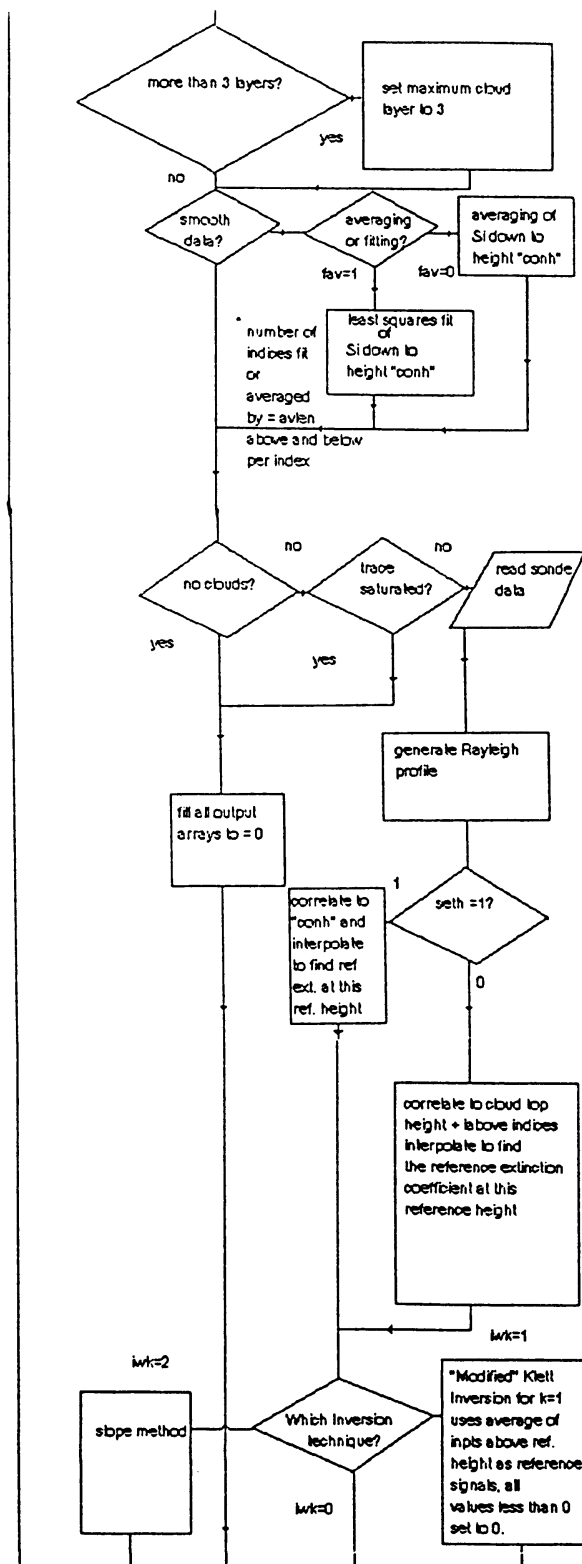


Figure 3.2: Flow chart of the KNMI2B2 software features and data processing scheme, part 2.

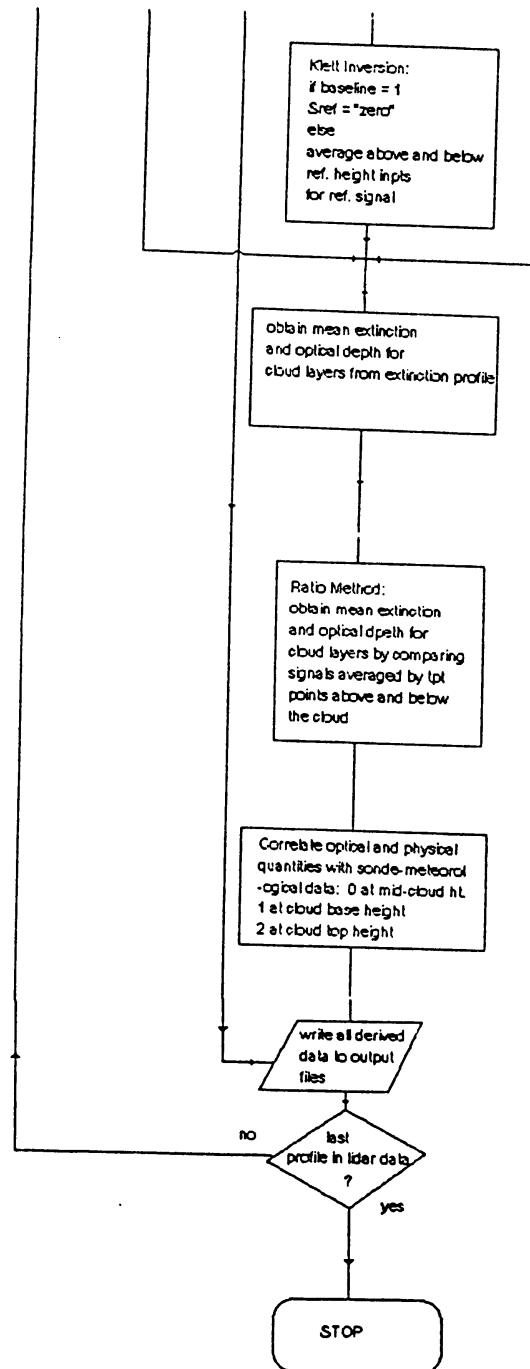


Figure 3.3: Flow chart of the KNMI2B2 software features and data processing scheme, part 3.

3.1 KNMI2B2 Operating Requirements: Support Files, Inputs and Formats

KNMI2B2 relies on four input files for its operation: para.dat, knmi2b.lis (the lidar and radiosonde data file list) and of course the lidar and radiosonde data themselves; para.dat has the following format:

```
npts,mpt,dpt,tpt,inpts,rrcor,lambda
100,3,3,5,20,1,1.064
rez,zero,nob,high,nlog,mixbit
40.00,-1.0e+20,1,1.0e+20,1,0
corrfa,k,xovlp,ieb,k,se,h,asw,conh,avlen
0.0,800.0,401,1.0,0,1,1500.0,20
nd,gain,nos,multi,offset,fav
0.0,0.0,250,1.,1.0e-30,0
thrush,ntot,iabove,iwk,isat,baseline,add,plusig
100.,14,2,0,1,1,1,10.0
```

Within the file each parameter required in the execution of the program is listed below the abbreviation used as the variable in the program itself and represent the following:

- npts: number of points in the lidar data per profile. The current version allows the user to select either 100 or 200 points [integer].
- mpt: number of points in the cloud base algorithm which are searched for to locate the subsequent peak signal corresponding a given cloudbase height in the cloud base height algorithm [integer].
- dpt: number of points fit used in determining the derivative in the cloud base height algorithm [integer].
- tpt: number of range interval points averaged above and below the cloud in obtaining an optical depth and a mean optical extinction value using the ratio method. The algorithm will average the number of points available. Hence if the number of points above the cloud in question is less than *tpt*, then it will use the number of points available [integer].
- inpts: number of points that the signal will be averaged above the cloud in order to obtain an adequate signal-to-noise ratio in the reference height

data The algorithm will average the number of points available. Hence if the number of points above the cloud in question is less than tpt , then it will use the number of points available [integer].

- rrcor: selects between removing range correction from lidar data (1) before processing or to not remove it (0) [integer].
- lambda: this is the wavelength used in the lidar system given in μm . This data is used to calculate the Rayleigh backscatter cross-section in the reference extinction coefficient calculation [38].
- rez: vertical resolution of the lidar system [real].
- zero: lowest possible value from the lidar data [real].
- nob: number of individual profiles to average over in order to obtain a sufficient SNR (no longer fully implemented, set to 1) [integer].
- high: highest possible value the optical extinction can have. Used in the inversion to account for cases where a zero occurs in the denominator (must be $\gg 1$, usually set to about 10^{+20}) [real].
- nlog:selects between using the logarithm of the backscatter signal (1) or the linear value (0) in the cloud base algorithm. For I.R. data set to 1 [integer].
- mixbit: selects between correlating meteorological measurements with cloud base(1), mid(0) or top (2) height [integer].
- corrfak: factor which sets the rejection criteria in the cloud base algorithm. This factor that determines the sensitivity of the algorithm. Normally low corrfak values tend to trigger on noise spikes, whereas high corrfak will not recognize weak cloud layers. It is described in the previous chapter in greater detail. for our data we have obtained satisfactory results with corrfak set to 0. [real].
- xovlp: overlap altitude height [height rejection criteria, for region of initial transmitter-receiver field-of-view (FOV) intersection.] (usually set between 500-800) [real].
- ieb: total number of complete profiles or traces to be read from the lidar data file [integer].

- *k*: backscatter to extinction ratio exponent, usually set to 1.
- *seth*: used in conjunction with the variable *conh*. When set to 1, it instructs the program to begin inverting the data from *conh* downwards [integer].
- *asw*: When set to 1, this parameter instructs the program to average from the top most range interval down to and stopping at the height specified by *conh* described below. The averaging is from point to point signals values adjacent in range over the number of intervals on either side of a given point specified by *avlen* described below. If *fav* (described below is set to 1, then a least squares fit is performed of *em avlen* points (up to 5 points only advised) instead of averaging. If set to (0) no averaging or fitting is performed [integer].
- *avlen*: specifies the number of intervals on either side of a given point that are averaged or fitted (see also *asw*, *avlen*, *fav*) [integer].
- *conh*: the confidence height is the highest possible altitude at which the user is confident of the signal to noise ratio. This setting specifies the height at which the program stops averaging (starting at the topmost range height downwards) to terminate averaging signals adjacent in range or the range at which to begin inverting when used with the parameters *asw*, *seth* or *fav*, as previously described [integer].
- *nd*: neutral density (optical) filtering applied during collection of data [part of cloud base algorithm rejection criteria].
- *gain*: currently not in use (set to 0).
- *nos*: number of shots collected and hardware averaged per profile (set to 250).
- *multi*: can be set to any number that the user wishes to multiply the entire profile by. This is useful extremely small values of signal where computational limits may interfere with optical inversions or cloud basing height location algorithms. Since all factors are divided out in the inversions, this value has no effect on our optical derived quantities [real].
- *offset*: any constant that the user wishes to add to the entire profile [real].

- fav: selects between least-squares fit (1) and simple averaging (0) of the signal from the topmost range height down to the height specified by the parameter *conh*. Must be used with *asw* (see above) set to 1 [integer].
- thrush: currently not in use (set to 0).
- ntot: total number of points in the sonde data [integer].
- iabove: number of points above the cloud top to set the reference height for the Klett Inversion as [integer].
- iwk: selects between a standard implementation of the far end (*Klett*) (set to 0) a modified algorithm for $k = 1$ described in the previous chapter by the Eq. 1.14 and suggested by W. Steinbrecht (set to 1) and the *slope method* (set to 2) inversions for obtaining the optical extinction profiles [integer].
- isat: selects whether or not to invert (0) or to disregard and not invert saturated data [integer].
- baseline: selects whether or not to invert using an average of the actual signal determined by inpts (0) or to use the value specified by the parameter *zero* as the value for the reference signal (1). This is useful only if the signal value at the reference height is known [integer].
- add: selects between background addition of the lowest value (negative) signal plus and offset specified above when on (1) or to not add any constant to the signal (0) [integer].
- plusig: user specified amount that can be added to the calculated Rayleigh extinction value [real].

3.2 KNMI2B2 Input/Output File Formats:

KNMI2B2 outputs five data files the names of which are specified in the third to seventh lines of the file list known as *knmi2b.lis*. The first two lines are input file names; *knmi2b.lis* has the following format:

```
93216riv.dat
9321600.dat
93216clb.dat
```

```

93216opt.dat
93216op2.dat
93216mix.dat
93216and.dat
93216tru.dat
93216nrc.dat
93216riv.t

```

The first line specifies the lidar backscatter file to be read, in the format: rows of 100 data points, 6 integer digit wide ASCII data separated by single spaces between points. The second line indicates the name of the sonde file for that day, in the format:

```

1x,pr,1x,ht,1x,tp,2x,rh,2x,dp,2x,wd,3x,wv

```

where,

nx: n character space(s)

pr: pressure in millibars in real 6 digit wide, 1 decimal place format.

ht: height in metres in integer 5 digit wide format.

tp: temperature in degrees Celsius in real 5 digit wide, 1 decimal place format.

rh: relative humidity in percent in integer 2 digit wide format.

dp: dew-point temperature in real 5 digit wide, 1 decimal place format.

wd: wind direction in integer 3 digit wide format.

wv: wind velocity in real 4 digit wide, 1 decimal place format.

The third line specifies the name of the output file containing the cloud base height algorithm [30] derived products in the format:

```

cbh 1, prh 1, ath 1, cbh 2, prh 2, ath 2, cbh 3, prh 3, ath 3

```

where, cbh x: cloud base height layer x

prh x: peak return height layer x

ath x: apparent top height layer x

All in metres and in real numbers format, 7 digit wide, no decimals.

The fourth line specifies the name of the output file containing all the optical extinction profiles in rows of 100 data points 10 digits wide, exponent with 3 decimal places.

The fifth line specifies the name of the output file containing the derived optical properties in the format:

`nl,op1,op2,op3,me1,me2,me3`

`nl`: number of cloud layers detected in a given profile.

`opn`: optical depth for cloud layer `n`.

`men`: mean optical extinction for cloud layer `n`.

All derived from integrating the extinction profile generated using the Klett inversion algorithm over the cloud layer [21].

The sixth line specifies the name of the output file containing the meteorological parameters read in from the sonde data correlated with the clouds optical and geometric properties at the cloud base, mid or top height in the following format:

`ht,1x,ct,1x,od,1x,me,2x,tp,1x,rh`

`nx`: `n` character space(s)

`ht`: base, mid-cloud or top height in metres in real 7 digit wide, no decimal place format.

`ct`: cloud geometric thickness in metres in real 7 digit wide, no decimal place format.

`od`: optical depth, in real 10 digit wide, 3 decimal place format.

`me`: mean optical extinction in 1/km, in real 10 digit wide, 3 decimal place format.

`tp`: temperature in degrees Celsius in real 8 digit wide, 1 decimal place format.

`rh`: relative humidity in percent in integer 4 digit wide format.

The seventh line specifies the name of the output file containing the identical optical extinction profiles in rows of 100 data points 10 digits wide, exponent with 3 decimal places specified in line four, but with each profile preceded by cloud base height algorithm [30] derived products in the format described for the file specified third line for that given profile.

The eighth line specifies the name of the output file containing the derived optical properties in the format:

`nl,op1,op2,op3,me1,me2,me3`

nl: number of cloud layers detected in a given profile in a 2 wide integer.
opn: optical depth for cloud layer n in exponent 10 wide, 3 decimal place format.
men: mean optical extinction for cloud layer n in exponent 10 wide, 3 decimal place format.

All derived from ratioing the signal just above and below the intervening cloud.

The ninth line specifies the name of the output file containing the non-range corrected version of the original backscatter profile in the rows of 100 points formatted in real numbers, 7 wide, no decimals.

The tenth and final line specifies the name of the time index file provided by RIVM. This file also contains the signal saturation status flag. The program will skip the first 13 columns and read the single character in column 14 which is either a j or a n. j positive is and n means no saturation.

Although not necessary, it useful to adopt some sort of naming convention to keep track of these different files as has been demonstrated above.

3.3 Installing KNMI2B2 and CirrusWare

To install KNMI2B2 and the other CirrusWare software, place the installation floppy disk in drive A and type:

```
>A:\setup.bat
```

The software will be automatically loaded into a newly created directory called CirrusWare. To create an applications window simply run Windows, click on the file manager icon, locate TRY and KNMIED2 in the CirrusWare directory and drag them to the applications window or one that you have created for CirrusWare.

3.4 Tutorial

To become familiar with KNMI2B2 follow these steps:

If the package has been installed, and you are running the software from MS/DOS, change to the CirrusWare directory and ensure that the following files are present:

```

9321600.DAT
93216RIV.DAT
93216RIV.T
KNMI2B2.FOR
KNMI2B2.EXE
KNMI2B2.LIS
PARA.DAT
TRY.BAT
KNMIED2.BAT
EMACS.EXE
EMACS.HLP
EMACS.RC

```

The source code will be listed in KNMI2B2.FOR. To run the program, type

```
>try
```

at the DOS prompt. If you are running it under Windows 3.0, find the applications group:

CirrusWare

and click on try.

This batch file will delete any existing output files if they exist and open the file para.dat with a MicroEMACS editor. Change or adjust the parameters of interest as desired by moving the cursor, inserting text and using the delete keys as required. For more details on the editor use the < f6 > key to expand the help window while it is running.

To use the editor for any other application simply type:

```
C:\emacs < filename >
```

Once the necessary changes have been made, type < CTRL >-X-S to save the settings and < CTRL >-X-C to exit the editor and begin the program.

KNMI2B2 will display a short identification logo, followed by prompts pertaining to the trace it is currently analysing. A TRACE ANALYZED will appear as the analysis is completed for each trace. It will indicate that the process is complete when a

...it is finally DONE

appears. Upon examining the directory you have been running in you will find the following additional new files:

```
93216AND.DAT
93216CLB.DAT
93216MIX.DAT
93216NRC.DAT
93216OP2.DAT
93216OPT.DAT
93216TRU.DAT
93216PRO.DAT
```

These can now be graphically displayed using Origin as discussed earlier. This can be repeated as many times as necessary in order for you to become more familiar or optimize the program parameters for a particular data set.

You may decide you want to modify some part of KNMI2B2 at some point. In such case you can click on, in Windows, or type, in DOS:

```
>KNMIED2
```

This batch file launches the emacs editor to open the source code for KNMI2B2. Once edits have been made, saved and the file closed, and if the Microsoft MS-FORTRAN 5.1 Compiler is installed on your system, it launches the Programmers Workbench. To create the new executable, using the mouse, pull down the MAKE menu and click on MAKE KNMI2B2.

Once it is compiled and linked an executable will be created, if the code passes without errors. Exit the compiler using the `< ALT > - < F4 >` combination. You can now run the modified program.

3.5 Examples of KNMI2B2 Outputs:

The following figures have been produced from data processed by the the software package KNMI2B2.

The software package Origin by MicroCal Software Inc. a Windows 3.0 application has been used to present the data here. Grey-scale plots require the use of the 3D version of Origin. Please consult the documentation that accompanies Origin and MicroCal for more details.

Figure 3.4 is a grey-scale plot showing the backscatter intensity time series of the lidar returns for the day 93216 (August 4th, 1993) without range correction (file 93216nrc.dat).

Figure 3.5 shows a plot of the file 93216clb.dat, indicating the detected cloud base, peak signal return height and apparent cloud top height for this day also.

Figure 3.6, is a grey-scale plot of the optical extinction derived from the backscatter intensity for that day also, using the Klett Inversion, it is generated from the file 93216opt.dat [21]. Note the bands of high values along the top edge of the time-series. These are the result of overestimates in the inversion boundary condition. As discussed it expected that the effect such errors will dissipate and the resultant profile should be accurate to within 10% of the actual value below 1500m.

A time-series of the mean optical extinction and cloud optical depths can be generated from the 93216op2.dat or 93216tru.dat files. The former values are derived from the optical extinction profiles derived by using the Klett Inversion [21] whereas the latter are values derived by comparing the signal above and below the cloud (*ie. the ratio method*) as discussed in the previous chapters. By plotting the values of mean optical extinction or optical depth derived from both methods, against each other, the success of the inversion can be gauged. See Figures 3.7-3.8.

Finally, plots of cloud optical or physical data correlated with meteorological data measured by sonde that day can also be generated from the file 93216mix.dat. Figure 3.9 shows a scatter plot of cloud optical extinction is compared with temperature at mid cloud height.

Comparable parameters in the file 93216mix.dat as stated previously include: mid-cloud or base or top height, cloud geometric thickness, optical depth, mean optical extinction, temperature and relative humidity.

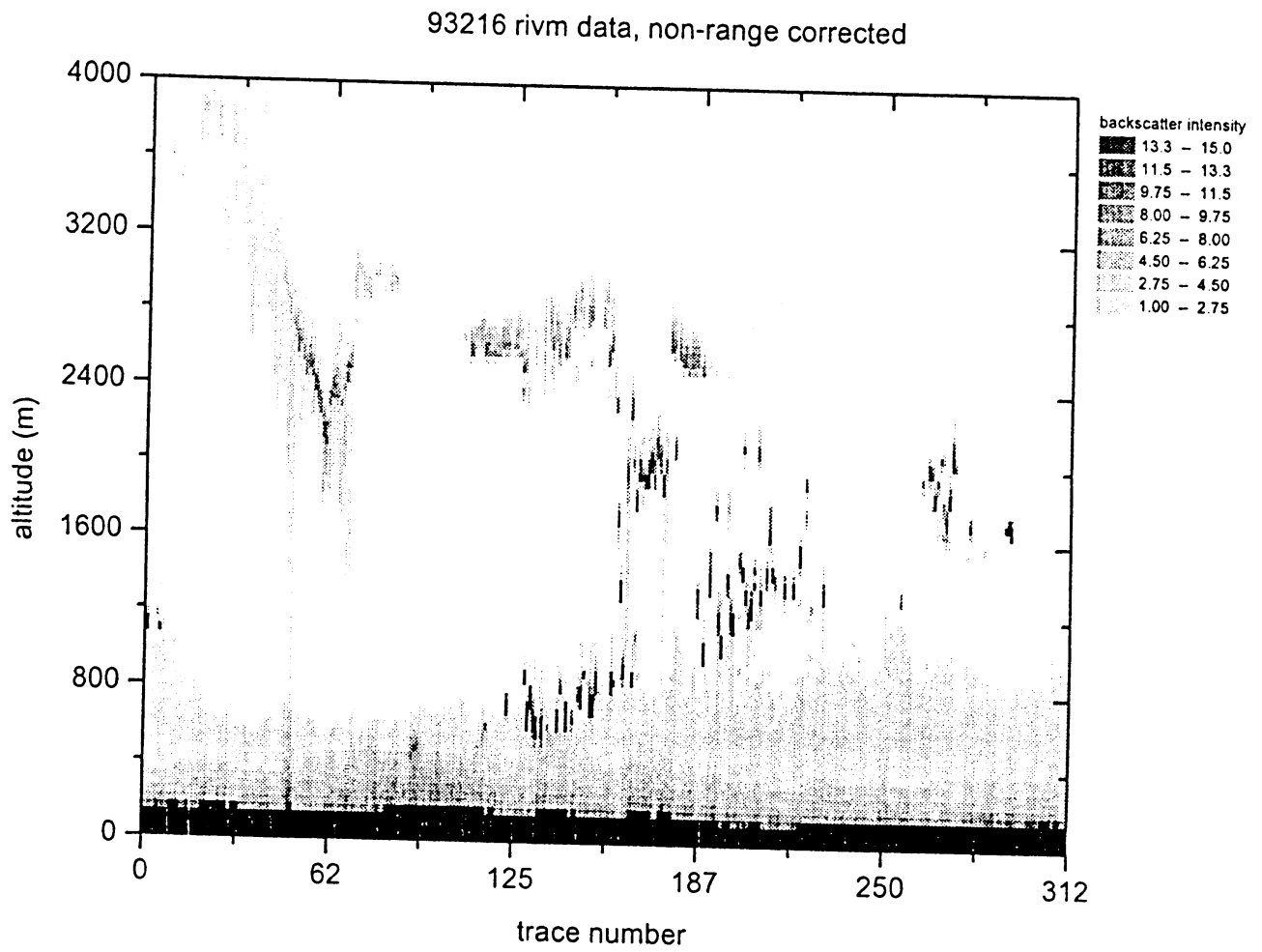


Figure 3.4: Grey-scale plot showing the backscatter intensity time series of the lidar returns for the day 93216 (August 4th, 1993) without range correction (files 93216nrc.dat)

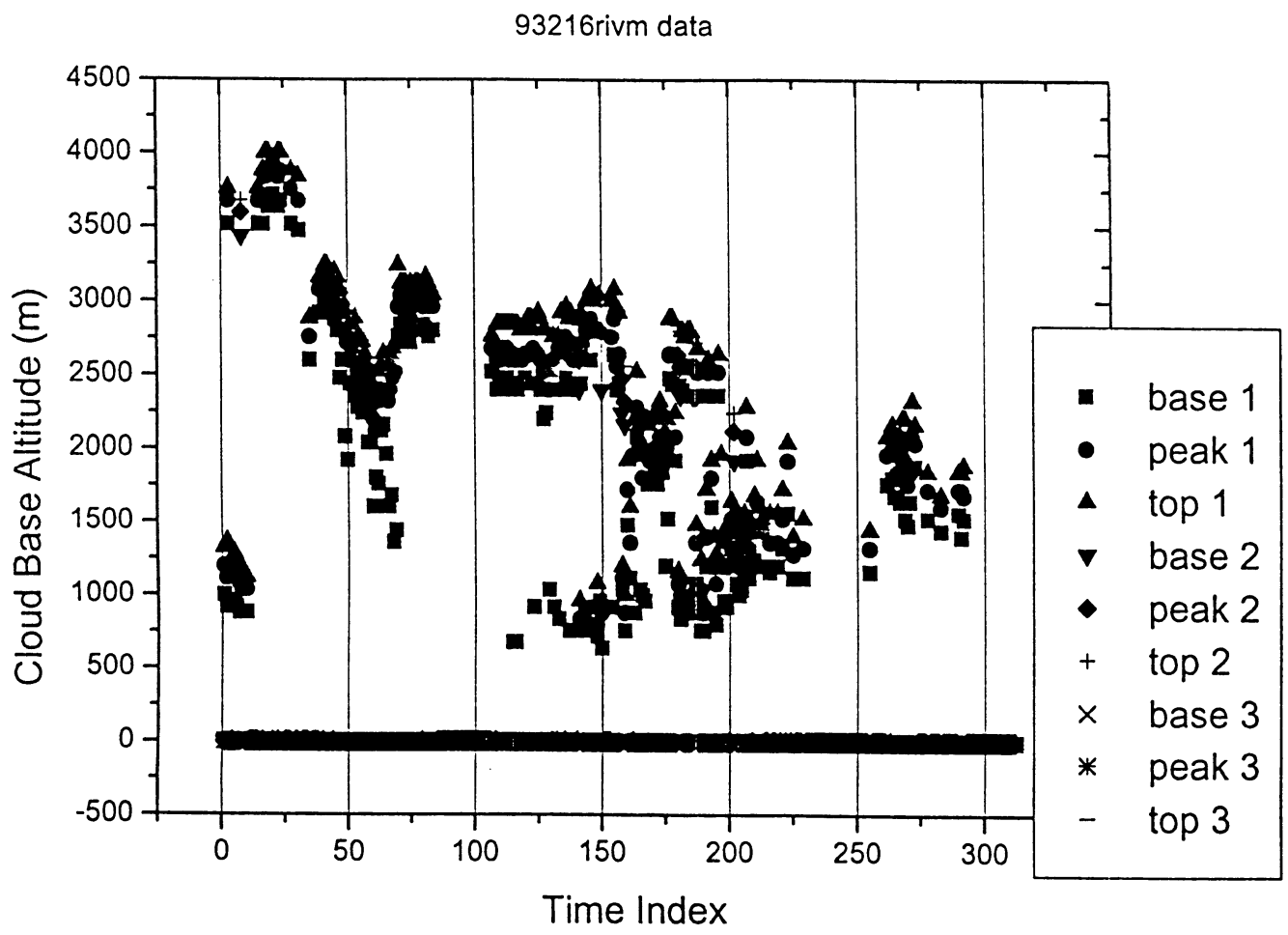


Figure 3.5: Plot of the file 93216clb.dat, indicating the detected cloud base, peak signal return height and apparent cloud top height for the day 93216 (August 4th, 1993)

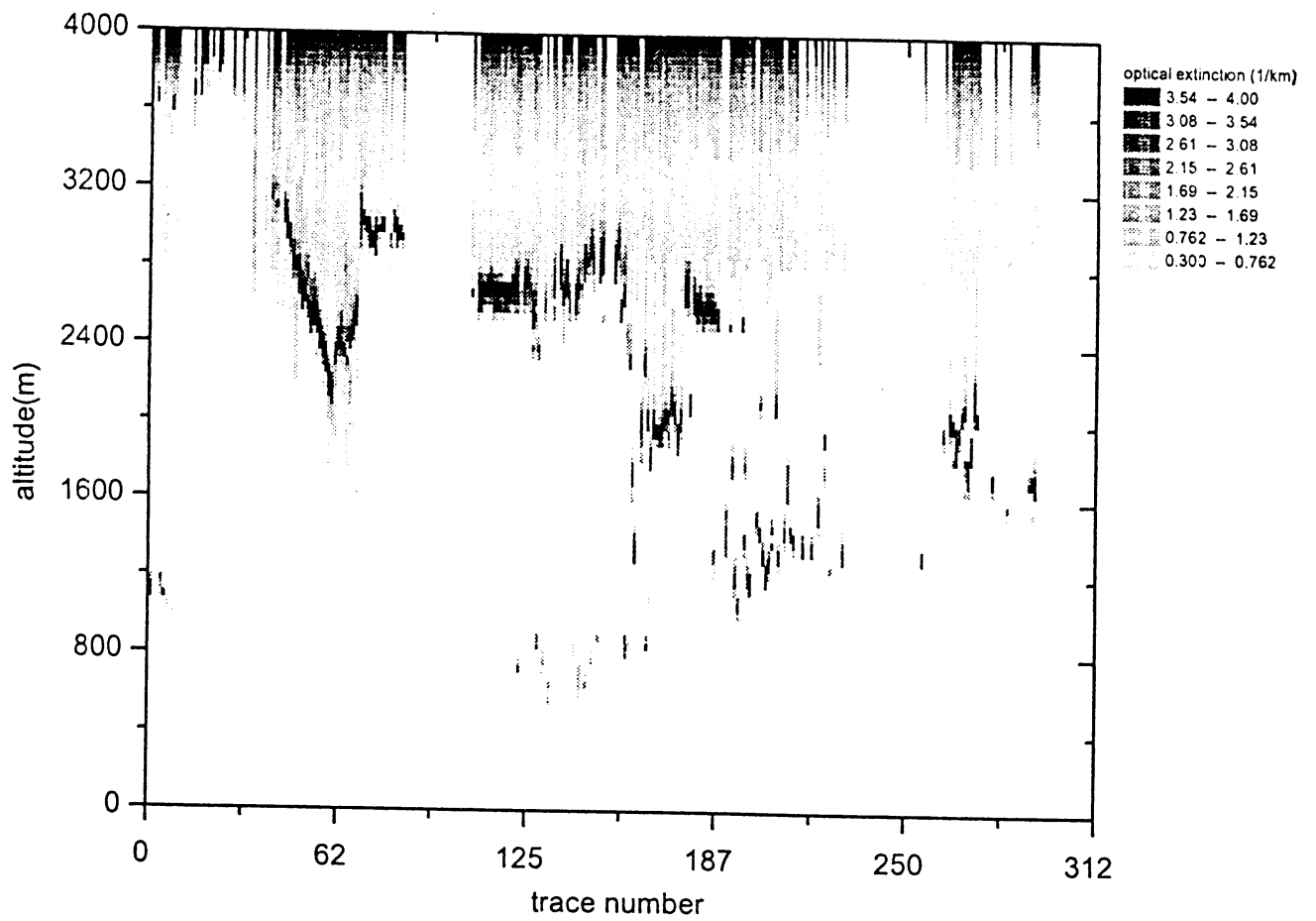


Figure 3.6: Grey-scale plot of the optical extinction derived from the backscatter intensity, for the day 93216 (August 4th, 1993), using the Klett Inversion

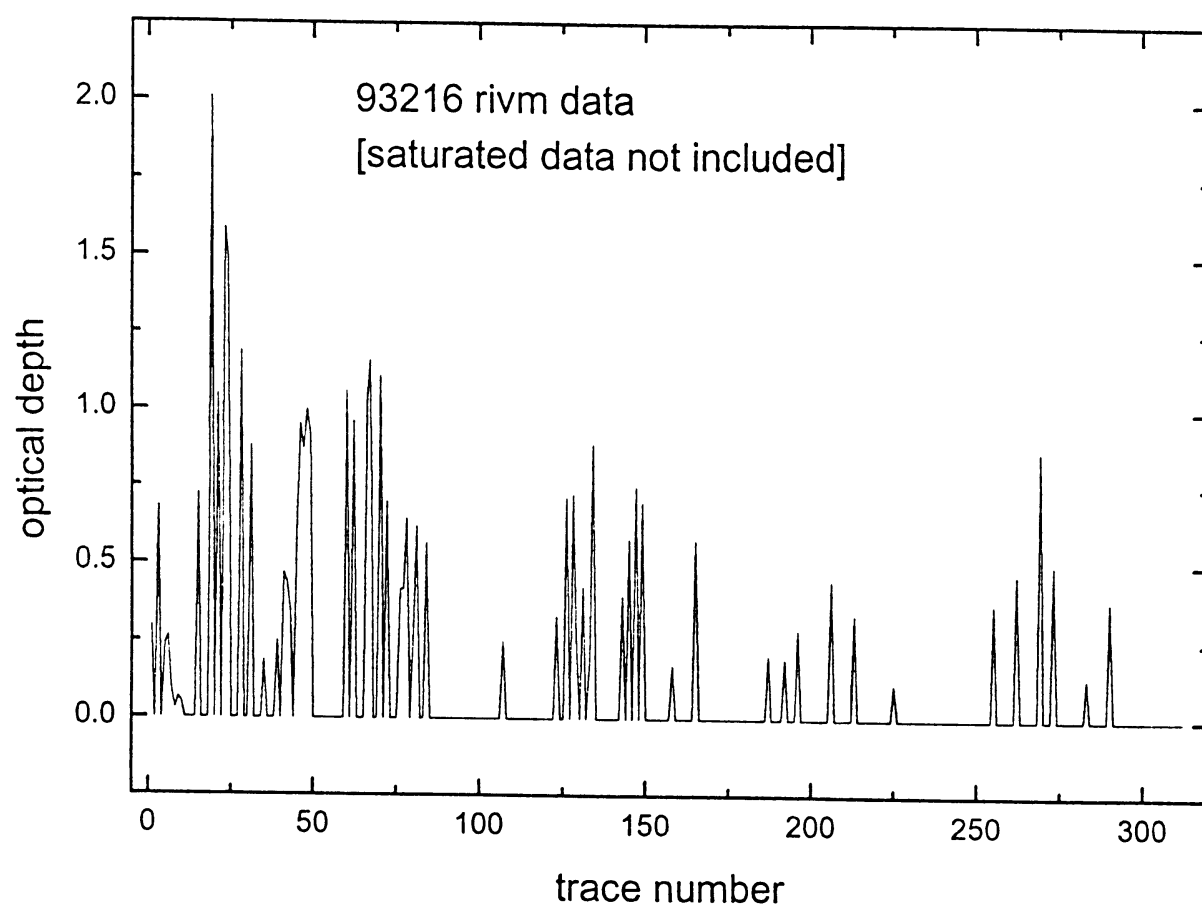


Figure 3.7: Time-series of the optical depth generated from the 93216op2.dat file

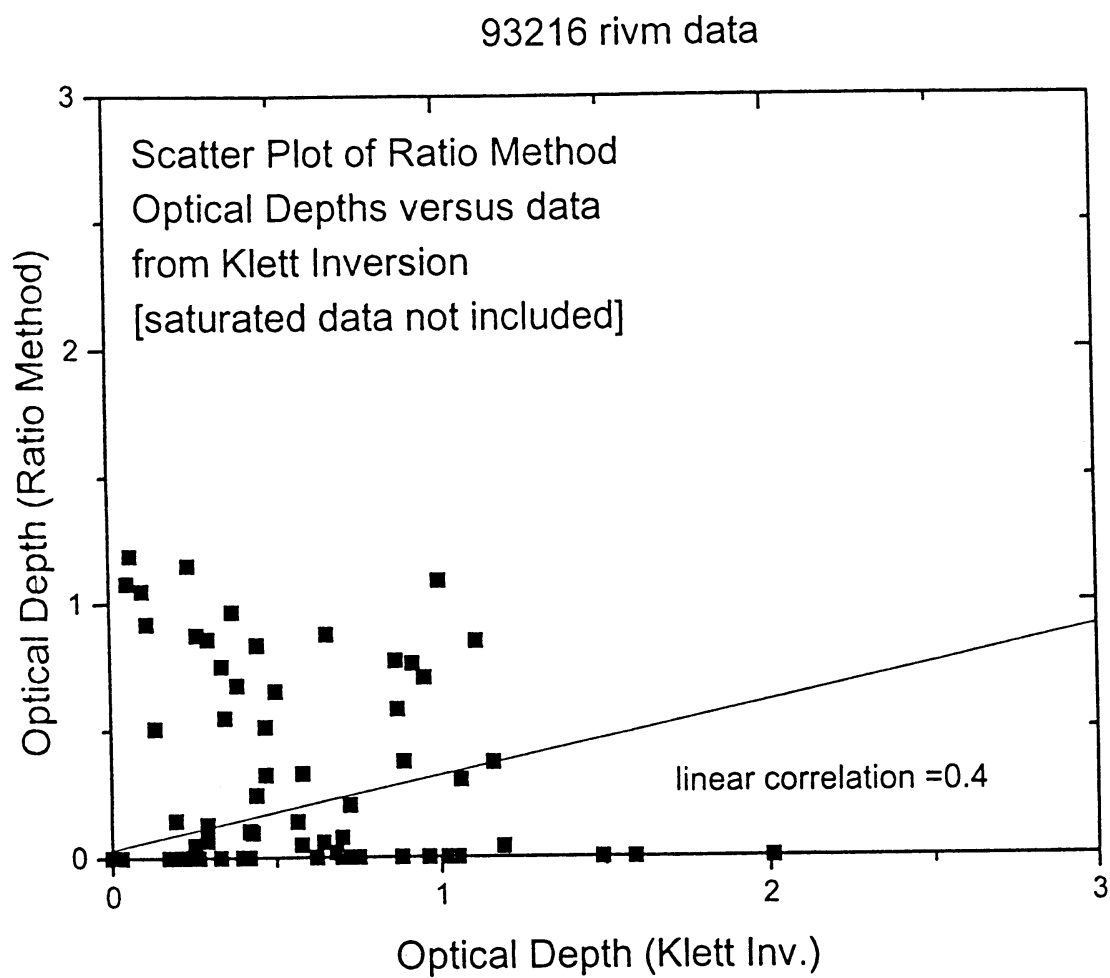


Figure 3.8: Scatter plot comparing the cloud optical depths generated from both 93216op2.dat and 93216tru.dat files

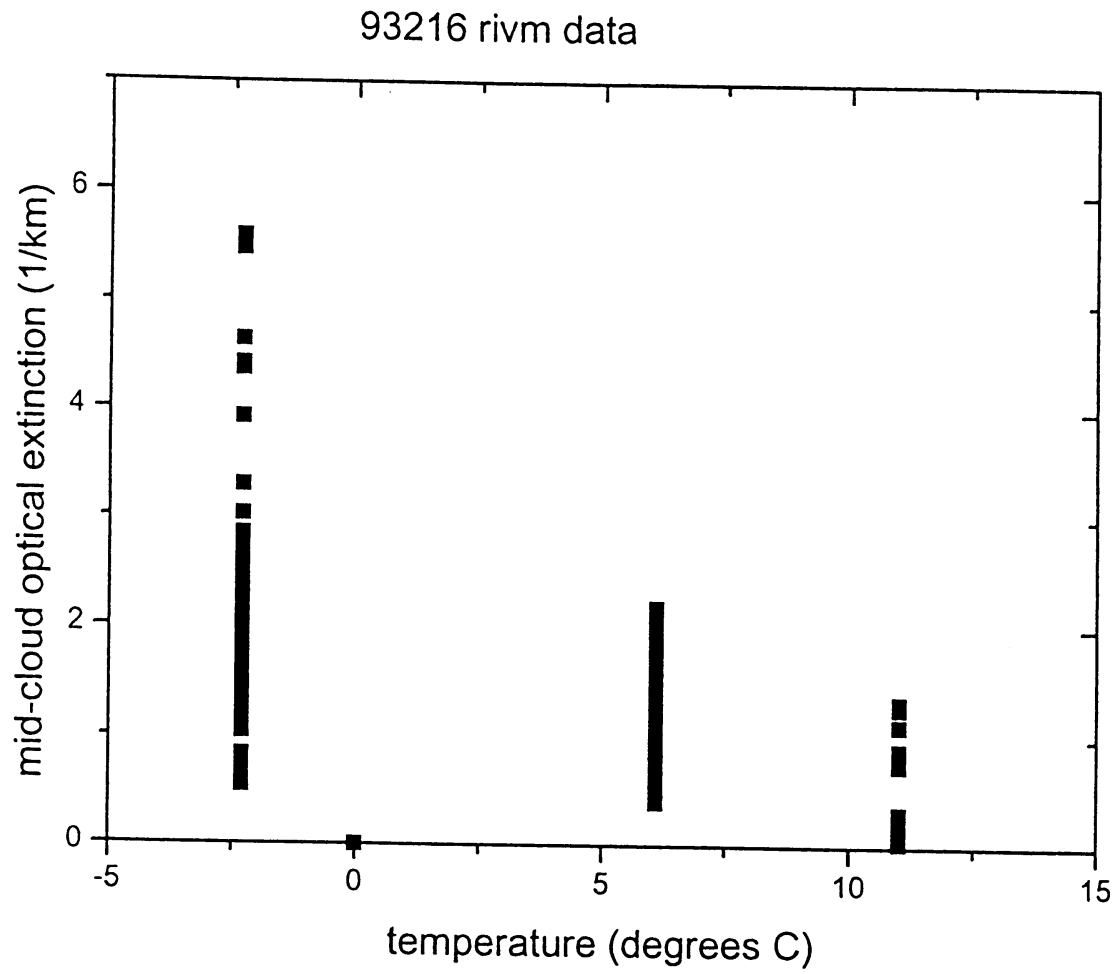


Figure 3.9: Scatter plot of cloud optical extinction compared with temperature at mid-cloud height

Chapter 4

Other Software

4.1 Lidar Simulation Software Set

To test the performance of the inversion algorithms used in our analyses, a set of smaller programs were developed to generate simulated extinction, lidar power and inverted profiles. These programs will be included in the CirrusWare directory under the subdirectory SIMU. All source codes have also been included.

RAYGEN3 generates a Rayleigh pure molecular atmospheric extinction profile either by assuming a lapse rate of $-6.75^{\circ}C/km$ and the hydrostatic pressure equation or from a given radiosonde profile. Cloud layers can be inserted as desired each with a user specified optical extinction value.

RAYGEN3 requires input parameters to be read from a file known as master2.dat which has the following format:

line 1: name of output file.

line 2: lapse rate or sonde generated profile for sonde (1).

line 3: the number of points in the sonde data.

line 4: the name of sonde data file.

line 5: how many points to generate the profile from using the lapse-rate/hydrostatic equation.

line 6: what resolution (metres) to generate the profile from using the lapse-rate/hydrostatic equation.

line 7: add noise (1) or skip (0).

line 8: desired signal-to-noise ratio.

line 9: how many cloud layers to add.

line 10-n cloud layers: mid-cloud height simulated cloud in metres, maximum extinction value at peak (1/km), thickness in metres

example:

```
bigclde.dat
0
15
9321600.dat
100
40
0
1.0e+20
3
3000.,1.0,200.
2000.,0.3,80.
1000.,0.2,320
```

The output has the following format:

```
1x,h,1x,s,1x,b,1x,k
```

where,

nx: n character space(s).

h: height in metres in integer 5 digit wide if generated from sonde, real 7 digit wide, 0 decimal place format otherwise.

s: optical extinction in 1/km as real 10 digit wide, 3 decimal place format.

b: backscatter coefficient in km as real 10 digit wide, 3 decimal place format.

k: backscatter to extinction coefficient ratio in real 10 digit wide, 3 decimal place format.

PGEN2 is an executable that generates a lidar backscattered power profile (or return) from a given extinction profile. Upon starting the program, it will ask the user to provide the following input parameters (typical values given):

extinction profile file name: 1cloud.dat

output filename: p1bcloud.dat

number of data points: 100

range resolution: 40.

starting value: 1.0e-6

multiplicative factor,

represents the geometric

and optical configuration
of the hypothetical lidar system
being simulated: 1.0e-6

It reads extinction profiles formatted identically as the output of RAYGEN3 and
write to the specified file the following output:

```
1x,range,1x,backscatter power
```

where,

nx: n character space(s)

range: height in metres real 7 digit wide, 0 decimal place format.

backscatter power: as real 10 digit wide, 3 decimal place format.

These values can be entered directly through the keyboard, following the on
screen prompts or through a redirect of an input file.

REVERT2 will invert the single backscattered profile generated by PGEN2
using the techniques utilized by KNMI2B2.FOR. It requires the following input
parameters, example filenames are given here:

```
name of file containing
simulated lidar profile
generated by PGEN2: p1bcloud.dat
name of file containing
simulated extinction profile
generated by RAYGEN3: 1cloud.dat
name of output file that
will contain cloud base height
and mean optical extinction and
optical depth information: det.dat
name of output file that
will contain the extinction profile
from the inverted data from
PGEN2: p1bclex.dat
```

It also requires a file known as para2.dat:

```
npts,mpt,dpt,tpt,inpts
100,3,3,0,0
rez,zero,nob,fax,high,nlog
```

```

40.00,13.6,1,1.0,1.0e+20,1
corrfak,xovlp,ieb,k,setref
0.0,0.0,401,1.0,0
nd,gain,nos,cban,baseline2
0.0,0.0,250,1,1480.0
thrush,ntot,iabove,iwk,baseline,add,plusig
100.,14,0,0,1,0.0,0

```

This file is almost identical to `para.dat` used for KNMI2B2, but with the following differences:

`isat`: is not specified or read here.

`fax`: is a multiplicative factor used to increase the absolute value of the signal so that slope changes can be easily detected by the cloud base algorithm. It is identical to *multi* in the `para.dat` file for KNMI2B2. It can be set to any number that the user wishes to multiply the entire profile by. This is useful extremely small values of signal where computational limits may interfere with inversions or cloud basing routines. Since all factors are divided out in the inversions, this value has no effect on our optical derived quantities [real].

`cban`: selects whether or not to use (0) or skip (1) the cloud base algorithm. If skip is selected then the program defaults to setting the reference inversion height at `npts`, or the highest range index, which is what is done if no clouds are detected [integer].

`nlog`: selects between using the logarithm (1) or linear (0) backscatter signal in the cloud base algorithm. For 1064 (I.R.) data use the logarithm [integer].

`baseline2`: defaults all values in the backscatter profile above the height it is set to to a constant value specified by *zero*. Unlike *baseline* these values are set to *zero* regardless whether or not they are greater than or less than [real].

`setref`: sets only the reference height signal point to the *zero* when it is set to 1 [integer].

The remaining parameters not listed here have the same function as and are described in the previous chapter in Section 3.1.

REVERT2 produces an output in the format, for example, in the file `det.dat`:

```

cbh1,ph1,ath1,cbh2,ph2,ath2,cbh3,ph3,ath3
n1,op1,op2,op3,me1,me2,me3

```

`cbhn`: cloud base height for layer `n`, real 7 digit wide, 0 decimal place format

phn: peak return height for layer n, real 7 digit wide, 0 decimal place format
 athn: apparent top height for layer n, real 7 digit wide, 0 decimal place format
 nl: number of cloud layers detected in a 2 digit wide integer.
 opn: optical depth for cloud layer n in exponent 10 digit wide, 3 decimal place format.
 men: mean optical extinction in 1/km for cloud layer n in exponent 10 digit wide, 3 decimal place format.

The file plbclex.dat, contains a single extinction profile in columnar format given as:

```
rng,sig,sigs,sigp,logsgnl
```

rng: range or height in metres in a real number 7 digit wide, no decimals.
 sig: optical extinction in 1/km in exponent 10 digit wide, 3 decimal place format derived using the Klett Inversion.
 sigs: optical extinction in 1/km in exponent 10 digit wide, 3 decimal place format derived using a modified Klett Inversion.
 sigs: optical extinction in 1/km in exponent 10 digit wide, 3 decimal place format derived using a Slope Inversion.
 logsgnl: log of the backscattered siganl in exponent 10 digit wide, 3 decimal place format.

4.2 Miscellaneous Support Software Included:

These programs can be found in the subdirectory MISC
 REPROC Prior to August 1st, 1993, data provided by RIVM was given in the following format:

```
Mail header (17 lines) [before April 12, 1993]
      date
...followed by the data set in the format:
      time stamp
10x12 data points, 120 points of which only the first 115 are
      valid]
```

Once launched, REPROC prompts the operator for the number of files to process, the header length as described above and the name(s) of the lidar file(s)

to reformat and the name(s) to write the reformatted data to, in pairs. This can be done manually through the keyboard, or by redirecting an input file such as through a batch job.

Once complete, REPROC reports:

>DONE!

to the operator

KEXTRA extracts individual traces from time series data files which are in the format of RIVM ASCII data or the optical extinction profiles generated from KNMI2B2 where each return profile or trace is written as a 100 data point row. When launched it prompts the operator for:

- name of file to read the data from.
- name of file to write the single trace output to.
- number of points in the data (prompted as *>npts*).
- range resolution and the most lowest value the data can equal(prompted as *>rez,zero*). If values are less than this value (*zero*) then they are set to it.
- total number of traces in the file
- number of the single trace to extract from that file.
- Is the file RIVM ASCII backscatter (1) or KNMI2B2 extinction, non-range corrected or processed averaged (0) data format?

These values can be entered directly through the keyboard, following the on screen prompts or through a redirect of an input file. Kextra writes them to single profile file in the format:

range, signal or extinction, range corrected signal or extinction

range: specified as a real seven digit, 2 decimal point value.

signal or extinction: data points are 10 digits wide, real with 3 decimal places and a single space is placed between columns.

CELTRAK this program extracts individual or groups of profiles from ceilometer data collected at Cabauw. The data normally has the format of 107 data

points per row as 2 integer digit wide ASCII data separated by single spaces between points. CELTRAK also requires the input file inst.dat which has the format show below:

```
93216348.DAT
93216348.CAT
107,401
1,312,0
```

The first line specifies the ceilometer file from which the data is to be read. The second line specifies the file to write to. The third and fourth lines have the following format:

```
npts,ieb
istart,notra,sw
```

where

npts: are the number of points in the data per profile.

ieb: the total number of profiles in the file.

istart: profile at which to begin extracting data.

notra: number of subsequent traces to extract.

sw: option to write out data in a single column (1) [only useful for single profiles] or rows (0).

CELTRAK outputs the data in the format of a 107 data point row in 2 integer digit wide ASCII data separated by single spaces between points or for the case of a single profile, in a 3 integer digit wide single column, depending upon the selection of *sw* by the user.

4.3 Software for Catalyst:

ALEX4 this executable converts the stored in Catalyst formatted binary files to ASCII in either columnar or row (as described for KNMI2B2) formats. Upon execution, it prompts the operator to:

```
>ENTER NAME OF FILE LIST
```

and example of a file list, dat.lst, is given below:

```
4.7,1,0,0,1
ALLHIGH.OUT
```

1000HIGH.001

1000Hout.001

1

From left to right the five values separated by commas on the first line are:

- range resolution in metres (4.7 in this case).
- number of signals to average over (1).
- number of indices or length of pretrigger to be used in generating
- a background to be subtracted from the rest of the actual signal (0 skips background subtraction).
- a switch that selects whether or not to range correct the data (1=range correct, 0=no range correction).
- another switch which determines whether to write the data in rows (0) or columnar data (1, only valid for single trace extraction).

If column format is selected then the profile is written in a single column from bottom to top, in 7 digit wide integer ASCII data format. Otherwise each return profile or trace is written as a 100 data point row 6 digit integer wide ASCII data.

The second line specifies the name of the file you wish to write the average of/or all the individual profiles from files you will look at.

Two filenames are and a the block number to be read are specified in groups of three or from the third to fifth lines for a single data file.

The third or first line of this cycle specifies the name of the file you wish to read.

The fourth or second line of this cycle specifies the filename you wish to write the data to if you are writing single traces from single trace files to single trace files. The fifth or third line of this cycle gives the number of the block to read (this is almost always 1).

Chapter 5

Conclusions

5.1 Diagnosis: Current Condition

The fundamental aims of this work have been three fold:

- Establishment of quality and limits of data
- Creation of a software environment for analysing cloud lidar data
- Insight into future research directions

These goals have been met and will hopefully be the beginning of a continued effort to understand and characterize clouds through the use of lidar technology.

As this software and documentation are in final development, the data being collected from the RIVM truck-mounted aerosol lidar is less than satisfactory. Among the problems include limited range which excludes a vast majority of the clouds of interest and places many of the tops of clouds recorded out of reach thereby making inversion for optical extinction impossible.

As the system is designed for the purposes of boundary layer aerosol detection, much of the cloud data is over the recording range of the digitizer and is “saturated” numerically. That is, a flattening at the maxima of the signal occurs. In addition, a problem from saturation of the solid-state detector has been observed. It is evident that high signals can induce afterpulsing in the avalanche photodiodes resulting in artifact signals above the cloud.

This also limits our ability to obtain reliable optical characteristics of clouds. We currently identify and obtain cloud base height algorithm [30] information on all signals and can disregard inverting saturated profiles for optical data, albeit the fact that they comprise large proportions of our currently available data.

Some residual overlap signal at the near end of the range leads to difficulties for the cloud base algorithm in locating the bottom signal of very low clouds. This strong return appears as part of the cloud signal hence the algorithm will identify it's increasing values as the bottom and regard it as part of a very expansive cloud. No satisfactory explanation has come from the RIVM regarding this problem.

Negotiations with the RIVM have been underway since this project was first proposed and included adopting a dual duty cycle for the system allowing it to record data at two different dynamic settings, one for clouds and the other for it's primary function, recording aerosol returns.

This has been abandoned in favour of an alternate approach utilizing an older aerosol system not currently in use. The following recommendations were discussed and agreed upon:

- System must be optimized-aligned for cloud-lidar measurements.
- The data acquisition will be set to collect 500 bins of data at a vertical resolution of 20 metres, thus extending the systems range capacity to 10km.
- Neutral density filter configuration will complement the dynamic range of system 1.
- new data acquisition software must be implemented.

After some delay these modifications were performed in time for the NASA-LITE (Lidar In-space Technology Experiment) project. Data has been collected in conjunction with the Space Shuttle overpasses as hoped, analyses are pending.

5.2 Future Plans: Prognosis

Even with such improvements to our measurements, the SNR for the molecular background is sufficiently low that obtaining a satisfactory range of optically invertable data with the available technology in the current manner will still be problematic. A possible remedy is to take more continuous measurements than the current 25 second and 4 minute rest duty cycle and averaging over longer time periods, thus increasing effective exposure time of the systems detectors as previously discussed. The RIVM group has observed some evidence of the faint molecular signal at and beyond 4000 meters using this technique [22].

Table 5.1: Comparison of Moisture Detection Capabilities Between the KNMI Cabauw Meteorological Tower and a potential Raman Water Vapour Lidar

Specification	Tower	Raman Lidar
Range	213m	3km (solar-blind [39]) up to 7 km (night-time[40][41])
Resolution	20m	5-150m (dependent on processing modality)
Accuracy	in-situ measurement	within $\pm 10\%$ when compared to radiosonde data above 20% *
Noise and Uncertainty	N/A	5-20%(solar-blind, depends on haze), 0.02%(night-time)
Cost	unavailable at this time [†]	approx. fl. 685.000,00 (\$ 500,000.00 CAN)[42]
Special Features		potential ability to measure other atmospheric species of interest, <i>ie. clouds, aerosol CO₂, etc., for limited extra costs.</i>

Proposals are currently pending approval to develop new systems in conjunction with the RIVM which will be better suited to obtaining cloud optical properties. These include a system with a source in the visible range, namely 532 nm. We expect such a system to have better SNR for molecular, providing us with better boundary conditions and hence more range in our optical inversions.

Of interest yet farther into the future, will be the possible foray into lidar remote sensing of water vapor or atmospheric humidity. The Royal Netherlands Meteorological Institute currently relies on a meteorological tower equipped with wet and dry bulb thermometers for atmospheric moisture measurements at the Cabauw meteorological site. Recent advances in optical, laser and signal processing technology have indicated a potential role for lidar (laser radar) in the routine measurement of atmospheric moisture. Tables 5.1-5.2 offers some comparisons between the two methodologies and together with some comments describing the advantages/disadvantages of either technology based on the results produced by research systems currently in operation.

Raman scattering is a weak molecular scattering process, whereby incident ra-

Table 5.2: Comparison of Moisture Detection Capabilities Between the KNMI Cabauw Meteorological Tower and a potential Raman Water Vapour Lidar, continued.

Specification	Tower	Raman Lidar
Other Considerations	relatively routine, low maintenance approximately 1 hour/week	currently only proven as a routine night time operation system, daylight system still limited mainly to research measurements. Low maintenance during routine operation, less than $\frac{1}{2}$ hour per week apart from data download. Will require periodically, a skilled technician for maintenance, mainly for the laser component of the system. Possibly 1 – 2 days every 2 – 3 months, depending on the duty cycle and laser specifications.
Temperature Limits	inoperable when freezing of wet bulbs occurs	independent of outside ambient temperature
Safety Requirements	N/A	with marine radar connected to the laser interlock, intrabeam hazard is eliminated, diffuse beam radiation is eyesafe.

diation is shifted by a fixed amount associated with rotational and/or vibrational-rotational transitions of the molecule of interest. The shift is as such particular to a molecule. It has been shown that the ratio between the Raman scattered energy from water vapor to nitrogen is proportional to the water vapor mixing ratio.

Raman vapor lidar utilizes these two factors in remotely obtaining water vapor profiles of the atmosphere.

For water vapor detection, there are currently three lidar methods being used. Conventional Raman at 347 nm is restricted to night-time use, due to the intervening solar background that will saturate the detection system. Solar blind systems use the 266 nm line, and are operational during the daytime, but have limited range by comparison. DIAL or Differential Absorption Lidar utilizes two absorption lines in the 720nm range and requires two incident wavelengths. By comparing the attenuation of one (on) to the other (off) it is possible to determine the concentration of an atmospheric species. It has been successfully proven effective in measurements of atmospheric ozone but has been shown prone to limitations for water vapor.

DIAL Water Vapour Lidar is competitive with Raman for tropospheric measurements but has reduced accuracy and precision with regards to boundary layer measurements. It also is prone to degradation in its vertical range resolution due to narrowing and absorption line shifts which result from decreasing pressure[43]. Although such systems have proven superior to the Raman-based lidars for regions above the troposphere with low resolution requirements, it is clear the for ranges and levels of precision required by the KNMI, Raman is the most effective methodology.

In terms of long term technical direction, moving towards an advanced remote sensing methodology would be beneficial for the KNMI in order to maintain a competitive lead with regards to practical standards of meteorological measurements. This is already the direction undertaken for such routine measurements such as cloud ceiling height [1].

Schwiesow [44] has discussed the potential for a completely self-contained, portable meteorological tower with a range of 1 km as a motivation for the meteorological community to move towards utilizing and helping to spur on the development of such technology. It is viewed that as the state of the art improves such a system will move from the many research instruments currently in use to a commercially packaged group of laser-based remote sensing devices. These systems will measure all the parameters that currently rely upon in-situ devices

mounted on an expensive and fixed location meteorological tower. Moreover all with greater precision and range. Lidar systems can currently profile atmospheric aerosols, temperature, wind direction and velocity, water vapor, cloud base height, apparent top height and ice-water phase content, ozone, CO_2 and a host of other atmospheric gases and other residents of interest.

At present, active remote sensing technologies can serve to complement a conventional meteorological tower array, but given the pace of growth in this field it is expected to marginalize the utility of the tower and eventually replace it.

5.2.1 Other Improvements: Far-End Extinction Coefficient Inversions with Range Variable Backscatter to Extinction Ratios

In applying Eq. 1.13 to solve Eq. 1.1, (the *Klett Inversion* [21]), it has been assumed neither the proportionality factor, C , in Eq. 1.7 nor the exponent k is constant.

Several observational and theoretical studies have shown that under a wide range of circumstances where backscatter from aerosols dominate molecular (*ie. hazy, cloudy, foggy conditions in the I.R.*), we may assume this relation is valid. Although it is possible formally, to account for the range dependence of C , this requires some independent knowledge of the spatial variation in the atmosphere which is generally not available [45].

If it is possible to obtain some functional dependence for the constant C , such that,

$$\beta = B(r)\sigma^k \quad (5.1)$$

where we have denoted the former constant in the relation C as the range dependent variable $B(r)$. This range dependent variable then has a functional dependence to $\sigma(r)$ which can be written in the form,

$$B(r) = f[\sigma_1(r)] \quad (5.2)$$

It is then possible to rewrite the *Klett Inversion* to accommodate for this variable.

$$\sigma = \frac{\frac{B_f}{B} e^{\frac{1}{k}(S-S_f)}}{[\sigma_f^{-1} + \frac{2}{k} \int^r \frac{B_f}{B} e^{\frac{1}{k}(S-S_f)} dr']} \quad (5.3)$$

given the reference value is known,

$$B_f = B(r_f) \quad (5.4)$$

We can utilize this improved solution by performing the basic *Klett Inversion* using Eq. 1.13 and deriving an initial guess for the extinction profile (denoted as $\sigma_1(r)$) in Eq. 5.2. This can be used to obtain values for $B(r)$ which can be used in the new form of the inversion above, Eq. 5.3.

This again is of course, only valid where the scatterers are relatively homogeneous and still assumes the single scattering case only.

A proposal may allow for a study to examine the effectiveness of this technique on real lidar data in the near future. This would be a verification of this technique using real data as compared to the original work which used data generated by other methods. Hence, it will be an extremely worthwhile and enlightening project.

References

- [1] P. Stammes, A.J. Feijt, A.C.A.P. van Lammeren, and G.J. Prangma. Tebex observations of clouds radiation–potential and limitations. Technical report, Koninklijk Nederlands Meteorologisch Instituut, De Bilt, The Netherlands, 1994. Technical Report TR–162, ISBN:90-369-2051-5 52 pp.
- [2] Alan I. Carswell. Lidar measurements of the atmosphere. *Canadian Journal of Physics*, 61(2):378–395, 1983.
- [3] Andrew Grant Cunningham. *Lidar Measurements of Optical Extinction in the Lower Troposphere*. PhD thesis, York University, North York, Ontario, June 1990.
- [4] C.M.R Platt, J.C. Scott, and A.C. Dilley. Remote sounding of high clouds ,vi, optical properties of midlatitude and tropical cirrus. *Journal of the Atmospheric Sciences*, 44:729–747, 1987.
- [5] A.I. Carswell. *Clouds: Their Formation, Optical Properties, and Effects*, chapter Laser Measurements in Clouds., pages 363–406. Academic Press, New York, New York, 1981.
- [6] Luc R. Bissonnette and Daniel L. Hutt. Multiple scattering lidar. *Applied Optics*, 29:5045–5046, December 1990.
- [7] Christian Werner, Jurgen Streicher, Hartmut Herrmann, and Hans-Gütner Dahn. Multiple-scattering lidar experiments. *Optical Engineering*, 31(8):1731–1745, August 1992.
- [8] K.E. Kunkel and J.A. Weinman. Monte carlo analysis of multiply scattered lidar returns. *Journal of the Atmospheric Sciences*, 33:1772–1781, September 1976.

- [9] J.V. Dave and J. Gadzag. A modified fourier transform method for multiple scattering calculations in a plane parallel mie atmosphere. *Applied Optics*, 9(6):1457–1465, June 1970.
- [10] Dave G. Collins, Wolfram G. Blättner, Michael B. Wells, and Henry G. Horak. Backward monte carlo calculations of the polarization characteristics of the radiation emerging from spherical shell atmospheres. *Applied Optics*, 11(11):2684–2696, November 1972.
- [11] W.L. Eberhard. Cloud signals from lidar and rotating beam ceilometer compared with pilot ceiling. *Journal of Atmospheric and Oceanic Technology*, 3:499–512, September 1986.
- [12] W.L. Eberhard. Physical concepts for interpreting signals from optical ceilometers. Technical report, NOAA/ERL/Wave Propagation Laboratory, Boulder, Colorado, 1986. NOAA Tech. Memo. ERL WPL-129, 52 pp.
- [13] N.E. Davis. The variation of very low cloud base with time and distance with height. *Meteorological Magazine*, 98:351–356, 1969.
- [14] Douglas Roewe and Kuo-Nan Liou. Influence of cirrus clouds on the infrared cooling rate in the troposphere and lower stratosphere. *Journal of Atmospheric Science*, 17:92–106, January 1978.
- [15] C.M.R. Platt. Remote sounding of high clouds:i. calculation of visible and infrared optical properties from lidar and radiometer measurements. *Journal of Applied Meteorology*, 18:1130–1143, September 1979.
- [16] C.M.R. Platt and A.C. Dilley. Determination of the cirrus particle single-scattering phase function from lidar and solar radiometric data. *Applied Optics*, 23(3):380–386, February 1984.
- [17] C. Martin R. Platt and Harshvardhan. Temperature dependence of cirrus extinction: Implications for climate feedback. *Journal Geophysical Research*, 93:11051–11058, 1988.
- [18] C.M.R. Platt and A.C. Dilley. Remote sounding of high clouds. iv: Observed temperature variations in cirrus optical properties. *Journal of the Atmospheric Sciences*, 38:1069–1082, May 1981.

- [19] C.M.R. Platt. Extinction in clouds. In *IRS.'84: Current Problems in Atmospheric Radiation, Proceedings of the International Radiation Symposium, Perugia, Italy*, pages 163–166, Hampton, Va., 1984. A. Deepak Publishing.
- [20] C.M.R. Platt, J.D. Spinhirne, and W.D. Hart. Optical and microphysical properties of a cold cirrus cloud: Evidence for regions of small ice particles. *Journal of Geophysical Research*, 94(D8):11151–11164, August 1989.
- [21] James D. Klett. Stable analytical inversion solution for processing lidar returns. *Applied Optics*, 20(2):211–220, January 1981.
- [22] Eric Visser. private communication, 1994. RIVM Remote Sensing Laboratory, Antonie van Leeuwenhoeklaan 9, Postbus 1, 3720 BA Bilthoven, (030)-74 91 11.
- [23] W.S. Steinbrecht. private communication, 1991.
- [24] A. Notari, U.N. Singh, T.D. Wilkerson, and W.C. Braun. Optical properties of high clouds. In *Digest of Topical Meeting on Optical Remote Sensing of the Atmosphere*, pages 210–211, Washington, D.C., 1990. Optical Society of America. volume 4.
- [25] World Meteorological Organization. *International Cloud Atlas, Manual on the Observations of Clouds and Other Meteors*, volume 1. World Meteorological Organization, Geneva, Switzerland, 1975 edition. WMO - No. 47.
- [26] Garry E. Hunt. *On the Diurnal Properties of Clouds from Geostationary Satellite Observations*, in: *Clouds: Their Formation, Optical Properties, and Effects*. Peter V. Hobbs and Ardash Deepak, editors; pages 281–313. Academic Press, New York, 1981.
- [27] Todd Berendes, Sailes K. Sengupta, Ron M. Welch, Bruce Wielicki, and Murgesh Navar. Cumulus cloud base height estimation from high spatial resolution landsat data: A hough transform approach. *IEEE Transactions on Geoscience and Remote Sensing*, 30(3):430–443, May 1992.
- [28] Kuo-Nan Liou. Influence of cirrus clouds on weather and climate processes: A global perspective. *Monthly Weather Review*, 114:1167–1199, June 1986.

- [29] David R. Dowling and Lawrence F. Radke. A summary of the physical properties of cirrus clouds. *Journal of Applied Meteorology*, 29:970–978, September 1990.
- [30] Shiv R. Pal, Wolfgang Steinbrecht, and Allan.I. Carswell. Automated method for lidar determination of cloud base height and vertical extent. *Applied Optics*, 31(10):1488–1494, April 1992.
- [31] Martin J.T. Milton and Peter T. Woods. Pulse averaging methods for a laser remote monitoring system using atmospheric backscatter. *Applied Optics*, 26(13):2598–2603, July 1987.
- [32] Norman Menyuk, Dennis K. Killinger, and Curtis R. Menyuk. Error reduction in laser remote sensing: combined effects of cross correlation and signal averaging. *Applied Optics*, 24(1):118–131, January 1 1985.
- [33] Jacek Karczewski. private communication, 1991. Optech Inc., 100 Wildcat Road., North York Ontario, M3J 2Z9, Canada Tel: (416) 661-5904, Fax: (416) 661-4168.
- [34] Walter Carnuth and Reinhold Reiter. Cloud extinction profile measurement by lidar using klett's inversion. *Applied Optics*, 25(17):2899–2907, September 1986.
- [35] Jan M. Mulders. Algorithm for inverting lidar returns: comment. *Applied Optics*, 23(17):2855–2856, September 1984.
- [36] Herbert G. Hughes, Jerry A. Ferguson, and Donald H. Stephens. Sensitivity of a lidar inversion algorithm to parameters relating atmospheric backscatter and extinction. *Applied Optics*, 24(11):1609–1613, June 1985.
- [37] Raymond M. Measures. *Laser Remote Sensing: Fundamentals and Applications*. Wiley-Interscience, Toronto, Canada, 1984.
- [38] Marcel Nicolet. On the molecular scattering in the terrestrial atmosphere: An empirical formula for its calculation in the homosphere. *Planet, Space Sci.*, 32(11):1467–1468, 1984.
- [39] D. Renaut and R. Capitini. Boundary-layer water vapor probing with a solar-blind raman lidar: Validations, meteorological observation and prospects. *Journal of Atmospheric and Oceanic Technology*, 5(5):585–601, 1988.


- [40] D.N. Whiteman, S.H. Melfi, and R.A. Ferrare. Raman lidar system for measurement of water vapour and aerosols in the earth's atmosphere. *Applied Optics*, 31(16):3068–3082, 1992.
- [41] S.H. Melfi and D. Whiteman. Observation of lower-atmospheric moisture structure and its evolution using a raman lidar. *Bulletin American Meteorological Society*, 66(10):1288–1292, October 1985.
- [42] Dr. Brent Smith. private communication, 1994. Optech Inc., 100 Wildcat Road., North York Ontario, M3J 2Z9, Canada Tel: (416) 661-5904, Fax: (416) 661-4168.
- [43] C. Weitkamp, M Riesbell, E. Voss, W. Lahmann, and W. Michaelis. Raman lidar for the measurement of height profiles of water vapor and carbon dioxide. Technical report, Alfred-Wegener-Konferenz on Ground Based Remote Sensing Techniques for the Troposphere, Hamburg, Germany, August 1986.
- [44] R.L. Schwiesow. Potential for a lidar-based, portable, 1 km meteorological tower. *Journal of Climate and Applied Meteorology*, 22:881–890, 1983.
- [45] James D. Klett. Lidar inversion with variable backscatter/extinction ratios. *Applied Optics*, 24(11):1638–1643, June 1985.

Addendum

Some recent changes have been made to KNMI2B2:

- The parameter *npts* (see page 44 of original document) selects as before, whether the lidar data to be read is 100 or 200 points in length. However, for *npts* equal to 200, the backscatter lidar data must be rows of 200 with the format of a real (or integer) number, 13 digits wide, no decimals. All output profile data, that are otherwise in rows of 100 in the data formats described in the original document, will remain in the same format except that the rows will now be 200 data points in length.
- If the parameter *rcorr* is chosen to be 0 (*off*), that is no range correction removal, then a range correction will be applied to the data written to file named on the 11th line of **knmi2b.lis** described below.
- With reference to page 47–48 of the original document, referring to the input file **knmi2b.lis**, an additional filename on the 11th line is now also read. This file (currently labelled **93216pro.dat** in the original **knmi2b.lis** file included with the package), contains profiles of the lidar backscatter data after whatever background addition, averaging and range-correction have been removed or added as selected by the user. The data are recorded in rows of 100 or 200 data points, in exponential format, 10 digits wide with 3 decimal places.

Regards,



Alexandre Y. Fong, M.Sc.
Cirrus Technology Consulting